

# The Shape of Hadrons

Constantia Alexandrou

*Department of Physics, University of Cyprus, P.O. Box 20537, 1678 Nicosia,  
Cyprus and The Cyprus Institute, 15 Kypranoros St., Nicosia, Cyprus*

Costas N. Papanicolas \*

*The Cyprus Institute, 15 Kypranoros St., Nicosia,  
Cyprus and Department of Physics, University of Athens, Athens, Greece*

Marc Vanderhaeghen

*Institut für Kernphysik, Johannes Gutenberg-Universität, D-55099 Mainz, Germany  
(Dated: October 30, 2018)*

This colloquium addresses the issue of the shape of hadrons and in particular that of the proton. The concept of shape in the microcosm is critically examined. Special attention is devoted to properly define the meaning of shape for bound-state systems of near massless quarks. The ideas that lead to the expectation of non-sphericity in the shape of hadrons, the calculations that predict it, and the experimental information obtained from recent high-precision measurements are examined. Particular emphasis is given to the study of the electromagnetic transition between the nucleon and its first excited state, the  $\Delta(1232)$ -resonance. The experimental evidence is critically examined and compared with lattice calculations, as well as with effective-field theories and phenomenological models.

PACS numbers: 13.40.-f, 25.30.-c, 14.20.-c, 12.38.-t, 12.39.-x

## Contents

		3. Large $N_c$ predictions	18
		4. Lattice QCD and chiral effective field theory	18
<b>I. Introduction</b>	1	<b>V. Conclusions</b>	19
A. Historical Development	2	<b>Acknowledgements</b>	20
B. Size and Shape in Classical and Non-Relativistic Quantum Mechanics	3	<b>References</b>	20
C. Size and shape in relativistic systems	4		
<b>II. Measuring and Calculating the Shape of Hadrons</b>	5	<b>I. INTRODUCTION</b>	
A. Empirical information for spin-1 particles: $W$ boson and deuteron	6	Hadrons are the smallest material objects in the universe known to be of finite size. The building blocks of the Standard Model, including leptons and quarks, are not known to have finite size with the smallest scale set by the experimental limit on the size of the electron, which is smaller than $10^{-18}$ m in diameter [1]. Hadrons are distinguished in two families: mesons, which are made out of a quark and an antiquark pair and baryons, which are made out of three quarks. Quantum Chromodynamics (QCD) does not exclude the possibility of other forms of hadronic matter such as di-baryons or pentaquarks, but none of these have been found thus far. The typical scale of a hadron radius is set by the well known charge radius of the proton, which is equal to $0.8768(69) \times 10^{-15}$ m [2]. The very concept of size, both classically and quantum mechanically, raises the issue of shape and it is therefore natural to inquire about the shape of hadrons. The shape of hadrons concerns microscopic objects at the scale of a femtometer ( $10^{-15}$ m).	
B. Measuring the shape of hadrons	7		
C. Calculating the shape of hadrons : lattice QCD	9		
<b>III. Experimental Evidence</b>	11		
A. Real Photon Measurements	12		
B. Electroproduction measurements	12		
C. Sensitivity, Precision and Estimation of Uncertainties	14		
<b>IV. The shape of nucleon and <math>\Delta</math> resonance : theoretical understanding</b>	14		
A. $\Delta$ charge densities : lattice QCD	15		
B. The electromagnetic $N \rightarrow \Delta$ transition in QCD	16		
1. Electromagnetic moments and densities	16		
2. Model descriptions of the $\gamma^*N\Delta$ transition	16		

\*corresponding author, email address: cnp@cyi.ac.cy

tion of its constituents or some of the extensive and therefore distributed properties, such as mass or charge, deviate from a spherical distribution, which is assumed to be the default distribution. However, hadrons are objects which are understood only within a quantum mechanical, relativistic framework. It is thus necessary to reexamine critically the concept of size and shape in the context of quantum mechanics and relativity before we address the question of the shape of hadrons. In parallel, we will also address the issue of how sizes and shapes are determined for particles of the microcosm.

Knowledge of the shape of the fundamental building blocks of the Universe, is not a curiosity, although it certainly comes close to being an example of the Aristotelian claim of the intrinsic human need to “know”. Experience from the determination and subsequent understanding of shapes of other objects in the microcosm such as those of atoms and nuclei, shows that this line of investigation is particularly fertile for the understanding of the interactions of their constituents amongst themselves and the surrounding medium. For hadrons this means the interquark interaction and the quark - gluon dynamics.

While the theoretical foundations describing hadrons as the smallest objects in the universe to which size and shape can be attributed are solid, the empirical knowledge concerning shape is limited and derives only from the detailed study of the transition to the first excited state of the proton, the  $\Delta^+(1232)$  resonance [3]. It is interesting to observe that while the determination that hadrons have size emerged early on, through the seminal work of R. Hofstadter and collaborators [4] and played a leading role in guiding hadron research ever since, the determination of shape has been elusive and continues to be very limited.

In the rest of this section we will review the development of the concepts of size and shape in classical and quantum mechanics with and without relativity, so as to establish the appropriate language needed to discuss the topic of “Shape of Hadrons”. This is necessary as hadrons are systems requiring a relativistic quantum mechanical description. In doing so, we will provide some historical background on how these concepts have developed.

### A. Historical Development

The issue of shape of subatomic particles arose most acutely in the case of nuclear physics. It is interesting to observe that historically the issue concerning the shape of atoms being non spherical never caused much surprise, perhaps because of the planetary (Rutherford) model, which intrinsically invokes non-spherical shapes. The discovery by Rabi and collaborators [5] that the deuteron had a static quadrupole moment and therefore its shape was not spherical was regarded as a major surprise. The discovery of deformation in the deuteron, and nuclei in general, was interpreted correctly as arising due to the existence of non-central (tensor) forces among nu-

cleons. Shortly afterwards, Gerjuoy and Schwinger proposed that trinucleon deformation (e.g.  $^3\text{H}$ ) could resolve some peculiarities in the spectroscopy of those systems [6]. This conjecture proved to be wrong - the effects were eventually understood to be due to mesonic degrees of freedom. The deuteron and trinucleon cases dramatically showed that understanding the shape of a subatomic particle requires a detailed knowledge of its constituents and it provides important information for their dynamics. Following the success of Rabi, the establishment and quantification of deformation through the measurement of the electric quadrupole moment of a particle was widely employed to map the systematics of deformation in atomic nuclei.

Unfortunately a number of misconceptions arose as a result of the successful use of the determination of quadrupole moments in inferring deviations from spherical shapes for atomic nuclei. The fact that the measurement of a quadrupole moment is possible only for systems (particles) possessing spin equal to one or bigger led incorrectly to the belief that the shape of particles possessing spin 0 or 1/2 cannot be determined. The impossibility to measure a quadrupole moment of such particles was mistakenly interpreted as signifying a spherical shape. It took more than two decades before this issue was clarified, primarily through the work of P. Brix and coworkers [7]. The realization that the determination of the intrinsic shape of a system is quite distinct from the ability to measure its quadrupole moment helped the field develop. Nuclear physicists developed new techniques to measure shapes that were also applicable to nuclei of spin 0 or 1/2. In cases where the rigid rotor (shape) approximation could be made, their excitation spectrum could be used to reconstruct the density [8].

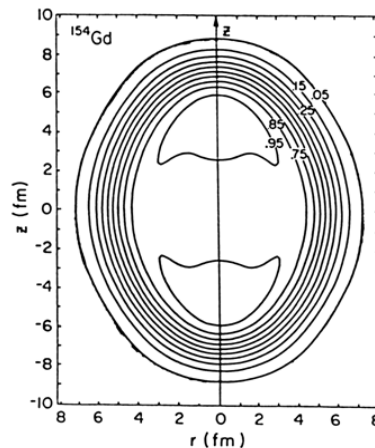


FIG. 1: Tomographic view of the deformed nucleus  $^{154}\text{Gd}$  derived from the study of the rotational bands of this nucleus using electron scattering [8]. The plot shows the contours of equal charge density revealing its shape. This spin zero nucleus has a vanishing quadrupole moment and therefore what is revealed through this reconstruction is its intrinsic shape.

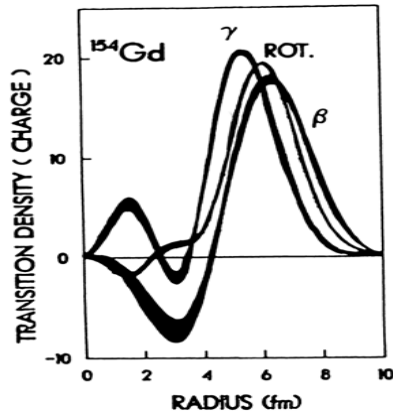


FIG. 2: The transition densities characterizing the moving charges involved in excitations in the deformed nucleus  $^{154}\text{Gd}$ , derived from the study of this nucleus using electron scattering [8], demonstrate that vibrations along the two axes of the ellipsoidal shape have different spatial extent.

In the seventies and eighties high resolution electron scattering, using this technique was used to map the shapes of the deformed nuclei in the rare earth and actinide regions of the periodic table. A superb example of the finesse of this tool is shown in Figs. 1 and 2. The reconstructed ground state charge density of the  $^{154}\text{Gd}$  spin zero nucleus [8] is mapped with high precision and the isodensity contours reveal vividly its deformation, as is seen in Fig. 1. Similarly the transition densities of  $^{154}\text{Gd}$ , shown in Fig. 2 provide a vivid geometric representation of the shape oscillations of the system along the long and short axes of symmetry again revealing its non-spherical charge distribution [8].

The understanding of the shape of nuclei led to a better understanding of nuclear structure and an appropriate language to describe a number of important nuclear phenomena. The development of the formalism of shape oscillations viewed as normal modes of the oscillating quantum liquid, nuclear matter, was a crucial milestone in the field of nuclear physics and indeed of physics. Modes of shape oscillations such as the “giant dipole oscillation”, the “breathing mode” or the “scissor’s mode” [9] have yielded valuable knowledge on a number of parameters characterizing nuclear matter. For instance, its compressibility, a parameter of critical importance in the understanding of supernova explosions, is derived from the study of the breathing mode of nuclei. Nuclear shapes and shape oscillations have also led to paradigms, which are driving the development in other fields of physics, such as the observation of a “scissor’s mode” in Bose-Einstein condensates in low temperature physics [10, 11].

It may appear from the preceding introductory comments that to inquire about the shape of an object possessing size is an obvious undertaking. However, it took more than twenty five years from the indication of the finite size of the proton to the inquiry about its shape. The

conjecture that hadrons would have non-spherical amplitudes was first made by Glashow in 1979 on the basis of non-central (tensor) interactions between quarks [12]. Glashow argued that this would resolve a number of inconsistencies that QCD was facing at the time if the constrain of sphericity of the shape of hadrons was relaxed. The conjecture of non-spherical hadrons originally was based on the premise that there is a color spin-spin interaction between the quarks [13], which is modeled after the interaction between magnetic dipoles in electromagnetism, the so-called “Fermi-Breit” interaction [14]. A few years later Isgur, Karl, and Koniuk wrote a seminal paper [15], which offered an impressive list of indirect empirical evidence for this hypothesis. However, in a remarkable similarity to the flawed trinucleon deformation hypothesis of Schwinger, due to the oversimplified description of the system, the non-relativistic shell model description of baryons (“tri quarks”) is now also found to be unable to quantitatively describe the deformation when solely invoking the color magnetic tensor interaction. The inadequacy of the non-relativistic description and of the phenomenological description of the constituents used (lack of mesonic degrees of freedom) are understood to be the principal deficiencies of this model.

In their paper, Isgur, Karl, and Koniuk singled out the quadrupole amplitude in the  $\Delta \rightarrow N\gamma$  transition as being a most sensitive test of this hypothesis. Of additional interest are the quark model calculations, which showed that the D-state admixtures caused by the color hyperfine interaction predict a non-zero neutron charge distribution and root-mean-square (RMS) charge radius [16–18]. These theoretical speculations induced concerted experimental and theoretical efforts to measure and calculate deviations from spherical symmetry (non-spherical amplitudes) in hadrons.

## B. Size and Shape in Classical and Non-Relativistic Quantum Mechanics

The concepts of both size and shape, because of their familiarity in everyday language, are often taken to be intuitively apparent, at least in classical physics. However, a careful examination reveals that this is not at all the case except for rigid objects with uniform density and sharp boundaries. The size of a hurricane or the size and the shape of nebula (e.g. the crab nebula) are not easy to quantify. However, the distribution in space and time of some extensive property of an object such as its mass or charge can uniquely and unambiguously be defined. Its mass density  $\rho(\mathbf{r})$  is uniquely defined and so is its variation in time  $\rho(\mathbf{r}, t)$ . In classical physics densities can be precisely defined and measured and their knowledge allows one to define a “size” and a “shape”. Moments of the density distribution are often quoted, which, in simple geometrical limiting cases, have the expected correspondence to the naive concept of size or shape. For

instance the second moment of the density distribution

$$\langle r^2 \rangle = \int d\mathbf{r} \cdot r^2 \cdot \rho(\mathbf{r}) \quad (1)$$

corresponds to the radius of a spherical body with uniform distribution  $\rho(\mathbf{r}) = \rho_0 \theta(R - r)$ .

For objects whose density distribution deviates from spherical symmetry it is obvious that higher moments will assume non-vanishing values. The first such moment whose non vanishing value indicates non-sphericity is the quadrupole moment  $Q_{ij}$  :

$$Q_{ij} = \langle Q_{ij} \rangle = \int d\mathbf{r} \cdot (3r_i r_j - r^2 \delta_{ij}) \cdot \rho(\mathbf{r}), \quad (2)$$

with  $i, j = 1, 2, 3$  denoting the spatial directions. It is worth noting that it is possible to have non-spherical distributions that have vanishing quadrupole moments.

The introduction of non-relativistic quantum mechanics and the implications of the uncertainty principle have influenced profoundly our understanding of the concept of size. Early on, with the aid of the ‘‘correspondence principle’’ it was realized that ‘‘size’’ could be expressed in terms of the RMS radius given by Eq. (1) where  $\rho(\mathbf{r}) = \psi^*(\mathbf{r})\psi(\mathbf{r})$  is the probability density expressed in terms of the wave function  $\psi(\mathbf{r})$  of the object. Likewise, the quadrupole moment of a system  $\langle Q_{ij} \rangle$  manifests deviation of its probability density from spherical symmetry.

### C. Size and shape in relativistic systems

The introduction of relativity does complicate matters. It is well understood that both the size and the shape of an object, are not relativistically invariant quantities: observers in different frames will infer different magnitudes for these quantities. Furthermore when special relativity is written in a covariant formulation, the density appears as the time (zeroth) component of a four-current density  $J^\mu = (\rho, \mathbf{J})$  (in units where the speed of light  $c = 1$ ).

Besides the relativistic kinematical effects, e.g. due to length contraction, the concept of size and shape in relativistic quantum systems, such as hadrons, is also profoundly modified as the number of constituents is not constant as a result of virtual pair production. Consider, as an example, a hadron such as the proton, which is probed by a space-like virtual photon, as shown in Fig. 3. A relativistic bound state is made up of almost massless quarks. The three valence quarks, which make up for the proton quantum numbers, constitute only a few percent of the total proton mass. In such a system, the wave function contains, besides the three valence quark Fock component  $|qqq\rangle$ , also components where additional  $q\bar{q}$  pairs, so-called sea-quarks, or (transverse) gluons  $g$  are excited, leading to an infinite tower of  $|qqqq\bar{q}\bar{q}\rangle, |qqqg\rangle, \dots$  components. When probing such a system using electron scattering, the exchanged virtual photon will couple to any quark, both valence and sea in the proton as shown

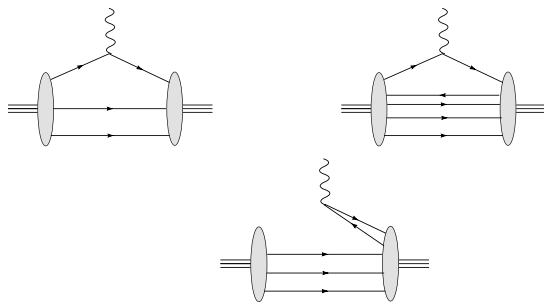


FIG. 3: Coupling of a space-like virtual photon to a relativistic many-body system, as a proton. Upper panel : diagonal transition where the photon couples to a quark, in the leading  $3q$  Fock component (left), or in a higher  $5q$  Fock component (right). Lower panel : process where the photon creates a  $q\bar{q}$  pair leading to a non-diagonal transition between an initial  $3q$  state and a final  $5q$  state in the proton.

in Fig. 3 (upper panel). In addition, the virtual photon, can also produce a  $q\bar{q}$  pair, giving rise e.g. to a transition from a  $3q$  state in the initial wave function to a  $5q$  state in the final wave function, as shown in Fig. 3 (lower panel). Such processes, leading to non-diagonal overlaps between initial and final wave functions, are not positive definite, and do not allow for a simple probability interpretation of the density  $\rho$  anymore. Only the processes shown in the upper panel of Fig. 3 with the same initial and final wave function yield a positive definite particle density, allowing for a probability interpretation.

This relativistic dynamical effect of pair creation or annihilation fundamentally hampers the interpretation of density and any discussion of size and shape of a relativistic quantum system. An interpretation in terms of the concept of a density requires suppressing the contributions shown in the lower panel of Fig. 3. This is possible when viewing the hadron from a light front, which allows to describe the hadron state by an infinite tower of light-front wave functions. Consider the electromagnetic (e.m.) transition from an initial hadron (with four-momentum  $p$ ) to a final hadron (with four-momentum  $p'$ ) when viewed from a light front moving towards the hadron. Equivalently, this corresponds with a frame where the hadrons have a large momentum component along the  $z$ -axis chosen along the direction of the hadrons average momentum  $P = (p + p')/2$ . One then defines the light-front plus (+) component by  $a^\pm \equiv a^0 \pm a^3$ , which is always a positive quantity for the quark or anti-quark four-momenta in the hadron. When we now view the hadron in a so-called Drell-Yan frame [19], where the virtual photon four-momentum  $q$  satisfies  $q^+ = 0$ , energy-momentum conservation will forbid processes where this virtual photon splits into a  $q\bar{q}$  pair. Such a choice is possible for a space-like virtual photon, and its virtuality is then given by  $q^2 = -\vec{q}_\perp^2 \equiv -Q^2 < 0$ , where  $\vec{q}_\perp$  is the transverse photon momentum (lying in the  $xy$ -plane). In such a frame, the virtual photon only couples to forward

moving partons, i.e. only processes such as those shown in the upper panel in Fig. 3 are allowed. We can then define a proper density operator through the + component of the four-current by  $J^+ = J^0 + J^3$  [20]. For quarks it is given by

$$J^+ = \bar{q}\gamma^+q = 2q_+^\dagger q_+, \quad \text{with} \quad q_+ \equiv (1/4)\gamma^-\gamma^+q, \quad (3)$$

where the  $q_+$  fields are related with the quark fields  $q$  through a field redefinition, involving the  $\pm$  components of the Dirac  $\gamma$ -matrices. The relativistic density operator  $J^+$ , defined in Eq. (3), is a positive definite quantity. For systems consisting of  $u$  and  $d$  quarks, multiplying this current with the quark charges yields a quark charge density operator given by  $J^+(0) = +\frac{2}{3}\bar{u}(0)\gamma^+u(0) - \frac{1}{3}\bar{d}(0)\gamma^+d(0)$ . Using such quark charge density operator, one can then define quark (transverse) charge densities in a hadron as [21, 22] :

$$\rho_\lambda(b) \equiv \int \frac{d^2\vec{q}_\perp}{(2\pi)^2} e^{-i\vec{q}_\perp \cdot \vec{b}} \frac{1}{2P^+} \times \langle P^+, \frac{\vec{q}_\perp}{2}, \lambda | J^+(0) | P^+, -\frac{\vec{q}_\perp}{2}, \lambda \rangle, \quad (4)$$

with  $\lambda$  the hadron (light-front) helicity. In the two-dimensional Fourier transform of Eq. (4), the two-dimensional vector  $\vec{b}$  denotes the quark position (in the  $xy$ -plane) from the transverse center-of-momentum (c.m.) of the hadron. It is the position variable conjugate to the hadron relative transverse momentum  $\vec{q}_\perp$ . The quantity  $\rho_\lambda(b)$  has the interpretation of the two-dimensional (transverse) charge density at distance  $b = |\vec{b}|$  from the transverse c.m. of the hadron with helicity  $\lambda$ . In the light-front frame, it corresponds with the projection of the charge density along the line-of-sight.

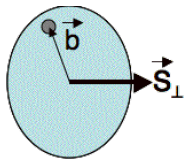


FIG. 4: Schematic view of the projection of the charge density along the line-of-sight (perpendicular to the figure), for a hadron polarized along the direction of  $\vec{S}_\perp$ . The position of the (quark) charge inside the hadron is denoted by  $\vec{b}$ .

The quark charge densities in Eq. (4) do not fully describe the e.m. structure of the hadron, e.g. for spin 1/2 the densities with  $\lambda = \pm 1/2$  yield the same information. We do know however that there are two independent e.m. FFs describing the structure of the nucleon. In general, a particle of spin  $S$  is described by  $(2S+1)$  e.m. moments. To fully describe the structure of a hadron one also needs to consider the charge densities in a transversely polarized hadron state, denoting the transverse polarization direction by  $\vec{S}_\perp$ . The transverse charge densities can be defined through matrix elements of the density operator

$J^+$  in eigenstates of transverse spin [23–25] as :

$$\rho_{T s_\perp}(\vec{b}) \equiv \int \frac{d^2\vec{q}_\perp}{(2\pi)^2} e^{-i\vec{q}_\perp \cdot \vec{b}} \frac{1}{2P^+} \times \langle P^+, \frac{\vec{q}_\perp}{2}, s_\perp | J^+ | P^+, -\frac{\vec{q}_\perp}{2}, s_\perp \rangle, \quad (5)$$

where  $s_\perp$  is the hadron spin projection along the direction of  $\vec{S}_\perp$ . Whereas the density  $\rho_\lambda$  for a hadron in a state of definite helicity is circularly symmetric for all spins, the density  $\rho_{T s_\perp}$  depends also on the orientation of the position vector  $\vec{b}$ , relative to the transverse spin vector  $\vec{S}_\perp$ , as illustrated in Fig. 4. Therefore, it contains information on the hadron shape, projected on a plane perpendicular to the line-of-sight. The matrix elements of the density operator can be written in terms of helicity amplitudes which in turn can be expressed in terms of the form factors. From  $\rho_{T s_\perp}$ , one can then straightforwardly define e.m. moments quantifying the shape. As an example, for a hadron with spin  $S > 1/2$ , and with transverse spin orientation  $\vec{S}_\perp = \hat{e}_x$ , the electric quadrupole moment is given by :

$$Q_{s_\perp} \equiv e \int d^2\vec{b} (b_x^2 - b_y^2) \rho_{T s_\perp}(\vec{b}). \quad (6)$$

These light-front densities require us to develop some new intuition, as they are defined at equal light-front time ( $x^+ = 0$ ) of their constituents. When constituents move non-relativistically, it does not make a difference whether they are observed at equal time ( $t = 0$ ) or equal light-front time ( $x^+ = 0$ ), since the constituents can only move a negligible small distance during the small time interval that a light-ray needs to connect them. This is not the case, however, for bound systems of relativistic constituents such as hadrons [26, 27]. For the latter, the transverse density at equal light-front time can be interpreted as a 2-dimensional photograph of a 3-dimensional object, reflecting the position of charged constituents at different times, which can be (causally) connected by a light ray.

## II. MEASURING AND CALCULATING THE SHAPE OF HADRONS

The determination of the shape of hadrons, interesting as it may be, presents a particularly difficult situation both theoretically and experimentally. The challenge lies in identifying the observables that can provide a characteristic signal, which can be experimentally accessed with sufficient accuracy and can be interpreted reliably to extract the information about shape. This has proved to be a particularly hard task for a number of reasons, which are discussed in this section.

It has been possible in the last decade to reach the appropriate sensitivity and technical maturity to obtain and analyze the data that can provide the first convincing information on the shape of hadrons. To interpret the data

in terms of hadronic structure quantities requires a reliable reaction framework. Such a reaction framework, as well as the interpretation and its connection to QCD, primarily through lattice gauge calculations, have advanced to maturity in recent years.

In this section we review and present these advances, the experimental methods, and the theoretical framework, which have allowed the first determination on the shape of hadrons.

### A. Empirical information for spin-1 particles: $W$ boson and deuteron

We start by discussing the empirical information on the e.m. moments of spin-1 particles, which are the particles with the smallest spin where a quadrupole moment can be measured. In nature, charged spin-1 particles include the  $W$  gauge bosons in the Standard Model of particle physics, the vector mesons in hadronic physics and the deuteron in nuclear physics. For a spin-1 system, it is customary to denote the three elastic e.m. form factors (FFs) as measured in elastic electron scattering by  $G_C$  (Coulomb monopole),  $G_M$  (magnetic dipole), and  $G_Q$  (Coulomb quadrupole), where the multipole nomenclature refers to a Breit frame interpretation.

From the empirical knowledge of the spin-1 FFs, one can map out the charge densities in a spin-1 particle of transverse polarization by working out the Fourier transform in Eq. (5), which yields monopole, dipole and quadrupole field patterns in the charge density [24]. The monopole field pattern corresponds to a circularly symmetric two-dimensional distribution for a spin-1 particle of fixed helicity. The dipole field pattern in the charge distribution is specific for a relativistic theory. Indeed, a magnetic dipole moment in a rest frame manifests itself as an electric dipole moment when seen by a moving observer, proportional to the vector product (velocity)  $\times$  (magnetic moment). The induced electric dipole moment (EDM) corresponding to the transverse charge densities  $\rho_{T s_\perp}$  of Eq. (5) for transverse spin projections  $s_\perp = 0, \pm 1$  is given by :

$$\vec{d}_{s_\perp} \equiv e \int d^2\vec{b}\vec{b} \rho_{T s_\perp}(\vec{b}). \quad (7)$$

For example, when the transverse spin projection  $s_\perp = 1$ , the expression for the electric dipole moment is [24]

$$\vec{d}_1 = -\left(\vec{S}_\perp \times \hat{e}_z\right) [G_M(0) - 2] e/(2M), \quad (8)$$

where  $M$  is the mass of the particle. Expressing the spin-1 magnetic moment in terms of the  $g$ -factor, *i.e.*  $G_M(0) = g$ , one sees that the induced EDM  $\vec{d}_1$  is proportional to  $g - 2$ . The same result was found for the case of a spin-1/2 particle [23]. One thus observes that for a particle without internal structure, corresponding with  $g = 2$  at tree level [28], there is no induced EDM.

The electric quadrupole field pattern in the transverse charge density  $\rho_{T s_\perp}$  yields a quadrupole moment, which is obtained, for  $s_\perp = 1$ , from Eq. (6) as [24] :

$$Q_1 = (1/2) [(G_M(0) - 2) + (G_Q(0) + 1)] (e/M^2). \quad (9)$$

For a charged spin-1 particle without internal structure, exemplified by the  $W$  gauge bosons of the standard electroweak theory, it is required that at tree level  $G_M(0) = 2$  and  $G_Q(0) = -1$ . For elementary particles, any deviations at tree level from these values would indicate new, beyond standard model, physics, and will show up in the presence of anomalous  $WW\gamma$  couplings, usually parametrized in terms of two new couplings  $\kappa_\gamma$  and  $\lambda_\gamma$ , appearing in an effective Lagrangian. In terms of those parameters, the  $W$  magnetic dipole and quadrupole moments take on the values [29] :

$$\mu_W = e/(2M_W) [2 + (\kappa_\gamma - 1) + \lambda_\gamma] \quad (10)$$

$$Q_W = -e/M_W^2 [1 + (\kappa_\gamma - 1) - \lambda_\gamma] \quad (11)$$

with  $M_W$  the  $W$ -boson mass. The Standard Model values  $G_M(0) = 2$  and  $G_Q(0) = -1$  equivalently correspond with  $\kappa_\gamma = 1$ ,  $\lambda_\gamma = 0$  at tree level. The measurement of the gauge boson couplings and the search for possible anomalous contributions due to the effects of new, beyond Standard Model, physics have been among the principal physics aims at LEP-II. They have been prominently studied in the  $e^+e^- \rightarrow W^+W^-$  process through an s-channel virtual photon exchange mechanism. The most recent Particle Data Group (PDG) fit for the anomalous  $WW\gamma$  couplings based on an analysis of all LEP data is given by [30] :

$$\kappa_\gamma = 0.973_{-0.045}^{+0.044} \quad \lambda_\gamma = -0.028_{-0.021}^{+0.020}. \quad (12)$$

One thus sees that present day information shows no evidence for anomalous  $WW\gamma$  couplings, confirming the point particle values  $G_M(0) = 2$  and  $G_Q(0) = -1$  for the  $W$  bosons, leading to vanishing induced electric dipole and quadrupole moments according to Eqs. (8, 9). It is thus interesting to observe from Eq. (9) that  $Q_{s_\perp}$  is only sensitive to the anomalous parts of the spin-1 magnetic dipole and electric quadrupole moments, and vanishes for a particle without internal structure.

For composite particles, it is the deviation from these benchmark values that indicate deformations of the states. A well studied example of a nuclear state is the deuteron. Its magnetic dipole moment is given by  $G_M^d(0) = 1.71$  [2], close to a spin-1 particle's natural (*i.e.* point-like) value. However, in contrast to the  $W$  gauge bosons, the deuteron has a large anomalous quadrupole moment. Its measured value is  $G_Q^d(0) = 25.84 \pm 0.03$  [31]. Its large value was interpreted to arise from the prominent role of the one-pion exchange tensor interaction. One also sees from Eq. (9) that the natural value  $G_Q(0) = -1$ , arising in a relativistic quantum field theory for a spin-1 point particle, only amounts to a few percent of the deuteron's total quadrupole moment. For an understanding of its static properties, the deuteron can therefore be

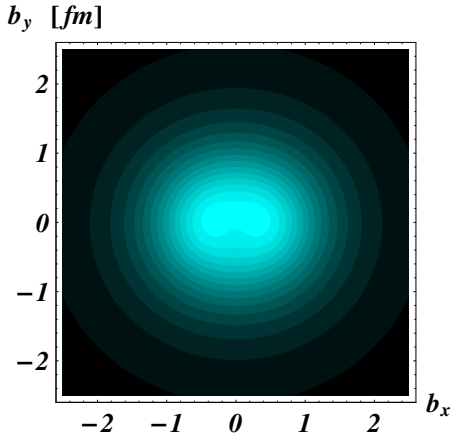


FIG. 5: Two-dimensional charge density  $\rho_{T1}$ , according to Eq. (5), for a deuteron polarized along the positive  $x$ -axis. The light (dark) regions correspond with largest (smallest) densities. The density is calculated from empirical information for the deuteron e.m. FFs [32]. Figure from Ref. [24].

considered, to a good approximation, as a non-relativistic bound state system.

In the case of the deuteron its three e.m. FFs have been separated experimentally [32], and it has been possible to determine the empirical charge densities. A pictorial result for the transverse charge density with transverse deuteron polarization  $s_{\perp} = 1$  is shown in Fig. 5. The quadrupole field pattern clearly displays a deformation along the axis of the spin ( $x$ -axis) together with a small overall shift of the charge distribution along the  $y$ -axis.

## B. Measuring the shape of hadrons

After the discussion of these two extreme cases, namely, on the one hand of a spin-1 point particle within relativistic quantum field theory, and on the other hand of a non-relativistic two-body system, we now turn our discussion to hadrons, such as mesons and baryons composed of light quarks.

Experimentally, accessing information that reveals hadron shape, even at the very rudimentary level that attempts only to check deviations from spherical symmetry, has proved very difficult for a number of reasons. There is only one stable hadron, the proton, and for this reason it is the only hadron that can provide a thick target for high luminosity precision measurements. The relatively long lived neutron either free or inside nuclei could provide a possible, but technologically far more difficult alternative. Its shape has not been explored so far. Both the proton and the neutron are unfortunately spin 1/2 systems and therefore cannot provide information about their intrinsic shape through the measurement of a static quadrupole or higher multipole moments. From the decuplet spin 3/2 baryons only in the case of the  $\Delta$  and the  $\Omega^{-}$  it is possible, in principle, to measure

their quadrupole moments or the transition quadrupole moments to some other state. The  $\Delta^{+}(1232)$  offers the most accessible case; however its exceedingly short lifetime prevents a viable, yet, experimental way to access its quadrupole moment. Nevertheless the magnetic moments of the  $\Delta^{+}$  [33] and  $\Delta^{++}$  [30] have been measured, albeit with very large errors. New experiments at MAMI are expected to yield a more precise measurement for the  $\Delta^{+}$  dipole moment. The dipole moment of the  $\Omega^{-}$  is more precisely measured and provides a benchmark for lattice QCD calculations [34], which in turn can predict its quadrupole moment. Vector mesons have a static quadrupole moment, which, if different from its natural value of -1, is a clear indication of a deviation from spherical symmetry. The  $\rho$ -meson is the lowest lying spin-1 resonance to test the deviation from spherical symmetry. However, experimentally it is again not feasible to measure. A beautiful example of what information lattice QCD can yield on hadron shapes is given in Fig. 6, which shows lattice calculations for the density-density correlator of the  $\rho$ -meson in the lab frame [35]. In the spin projection zero case, the  $\rho$ -meson displays a prolate (cigar-like) deformation in its rest frame. This conclusion is corroborated by a calculation of the  $\rho$ -meson quadrupole moment in quenched lattice QCD [36].

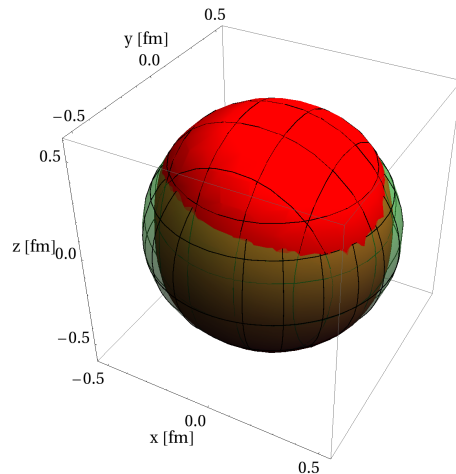


FIG. 6: Three-dimensional contour plot of the  $\rho$ -meson, of spin projection  $s_z = 0$ , density-density correlator (red surface), showing all positions where the correlator is reduced to half its value at the origin. As can be seen, by comparing to a sphere (green transparent surface) of radius of approximately 0.5 fm, the  $\rho$ -meson surface extends outside the sphere at the poles whereas at the equator is inside the sphere, showing the cigar-like  $\rho$ -meson shape.

Thus to measure the shape of hadrons, none of the “standard” and tested methods used in atomic and nuclear physics can be employed. The only viable path to study the nucleon shape remains the one originally proposed by Isgur and Karl, i.e. to measure the presence of resonant quadrupole admixtures in the  $\gamma^*N \rightarrow \Delta$  transition, which amounts to determining the off-diagonal

(transition) quadrupole moment. The theoretical framework of interpreting these measurements has matured in recent years, as will be reviewed below. The precision measurements of this transition provide the most reliable information we have today for deviation from spherical shape for the proton and/or the  $\Delta^+(1232)$  [3].

The experimental technique employed in the determination of the deviation from sphericity in the study of the de-excitation of the  $\Delta^+(1232)$  resonance is different than those discussed earlier. It involves the detection of the radiation pattern of the emitted radiation in the de-excitation of the excited state. The concept behind the technique derives from classical electromagnetism. The observed radiation pattern, its multipole content to be precise, reveals information about the shape of the radiating antenna. The radiation emitted in the de-excitation of the  $\Delta^+(1232)$  is primarily in the form of pions but a small (0.7%) branch of  $\gamma$  rays is also present. This technique of measuring shape rarely has been used in nuclear physics, principally due to the experimental complexity it presents. An important exemption is the study of the  $^{15}\text{N}$  excited states using this technique in an  $(e, e'\gamma)$  experiment, which demonstrated both the feasibility and accuracy of this method. The 6.33 MeV  $J^P = 3/2^-$  excited state of  $^{15}\text{N}$ , a  $J^P = 1/2^-$  nucleus, presents a case where a transition to it from the ground state with the same quantum numbers as the  $\gamma^*N \rightarrow \Delta$  can be studied. The experiment, where the C2 (Coulomb quadrupole), E2 (electric quadrupole) and M1 (magnetic dipole) FFs were isolated through the tagging of the decay radiation [37], offers a clear demonstration of the power of the technique. The experimental arrangement used is shown in Fig. 7, which clearly portrays the concept of this experimental technique. The virtual photon causes the excitation of the target nucleus and due to angular momentum and parity selection rules only magnetic dipole and electric quadrupole transitions are allowed; the decay radiation pattern allows to identify each admixture.

In the excitation spectrum of the nucleon the only isolated state is the  $\Delta^+(1232)$ , which thus allows us to employ the same type of measurement as in the 6.33 MeV isolated excited state of  $^{15}\text{N}$ . The  $\gamma^*N \rightarrow \Delta$  transition from  $J = 1/2$  to  $J = 3/2$  with no change in parity allows us to observe quadrupole E2 and C2 transition moments. It is however a mixed transition, which, in addition to the quadrupole amplitudes, involves the M1 (spin flip) amplitude that is the dominant one. The presence of resonant quadrupole strength signifies deviation from sphericity of the proton and/or the  $\Delta^+(1232)$ . Using the same experimental technique as in the case of  $^{15}\text{N}$  it is possible to isolate and measure the weak but important quadrupole amplitudes in the presence of the dominant M1 transition. Through the extensive study of the  $N \rightarrow \Delta$  transition, pursued during the last thirty years using real or virtual photon probes, an extensive body of data has emerged that convincingly demonstrates that the quadrupole amplitudes are substantial and far bigger than can be accommodated by a 'spherical' proton.

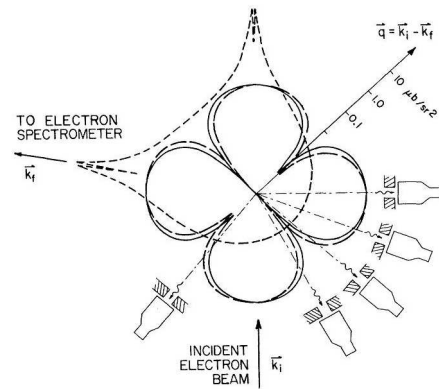


FIG. 7: The detection of the de-excitation radiation pattern from a system allows to isolate the contributing multipoles. The isolation of the multipole FFs was achieved for the first time in the  $^{12}\text{C}(e, e'\gamma)$  and  $^{15}\text{N}(e, e'\gamma)$  reactions where the E2 and M1 FFs were isolated through the tagging of the decay radiation [37]. The figure shows the radiation pattern and the isolated FFs for this transition in  $^{15}\text{N}$ .

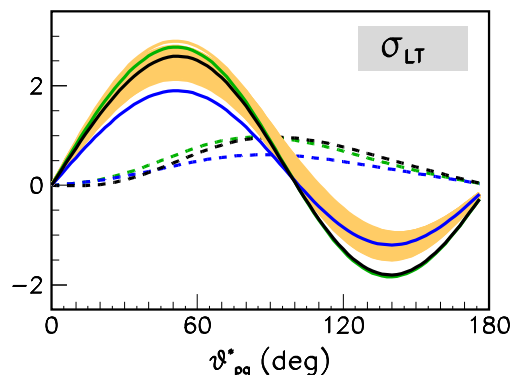


FIG. 8: The precise range of uncertainty that is allowed by the Bates and MAMI data for the  $\sigma_{LT}$  response of the  $p(e, e'p)\pi^0$  reaction, at  $Q^2 = 0.127 \text{ GeV}^2$  and at the position of the  $\Delta^+(1232)$  resonance, is shown as a function of the c.m. angle between the proton and virtual photon  $\theta_{pq}^*$ . Current phenomenological models (MAID [38] in black, Sato-Lee [39] in blue and DMT [40] in green) predict this satisfactorily within a  $2\sigma$  confidence level. The corresponding calculations for “spherical” nucleon and  $\Delta$  (dashed curves using same color coding for the various models) cannot describe the data; they are excluded to  $2\sigma$  confidence level.

Experimentally, the measurement of the small value of the electric or Coulomb quadrupole multipole becomes possible through its interference with the dominant magnetic dipole transition. This is shown in Fig. 8 which depicts the angular dependence of the longitudinal-transverse interference cross section ( $\sigma_{LT}$ ) for the  $p(e, e'p)\pi^0$  reaction on top of the  $\Delta^+(1232)$  resonance. The cross section  $\sigma_{LT}$  is overwhelmingly driven by the interference of the dominant transverse M1 amplitude with the longitudinal C2 amplitude. The experimentally



constrained region, by the Bates and MAMI data, is compared with phenomenological model predictions that attempt to describe the experimental data. It is evident that the model predictions (dotted curves) with resonant quadrupole amplitudes set to zero, which amounts to spherical solutions, are excluded with high confidence. The “deformed” model predictions, assuming negligible model error, are in agreement at the  $2\sigma$  level, with the empirical results. This comparison demonstrates that compelling experimental evidence nowadays exists supporting the conjecture of deformed hadrons. In particular, the above data demonstrate with very high confidence that spherical symmetry for both the nucleon and the  $\Delta^+(1232)$  is experimentally excluded. The experimental results for hadron deformation in the  $\gamma^*N \rightarrow \Delta$  transition will be discussed in more detail in Section III.

### C. Calculating the shape of hadrons : lattice QCD

Having seen clear experimental evidence for a non-spherical charge distribution in the  $N \rightarrow \Delta$  transition, we next examine whether this can be calculated and understood from QCD, the underlying theory of strong interactions.

QCD requires a new methodology in order to evaluate quantities related to hadron structure, the reason being that hadrons are bound state systems having a mass that is mostly generated by the interaction rather than by the sum of the mass of their constituents. Perturbative QCD has been very successful in describing high energy processes. On the other end of very low energy, chiral perturbation theory has provided the appropriate effective field theory framework for precise calculations of observables in terms of a small expansion parameter, such as an external momentum or pion mass. This framework provides a systematic expansion involving an increasingly large number of low-energy constants (LECs). The latter are free parameters, which are beyond the predictive power of the effective field theory. Some of these have been determined from phenomenological information, however, the vast majority remains unknown limiting the predictive power of chiral effective field theory. To calculate LECs from the underlying theory of QCD as well as to make predictions beyond a regime where a perturbative or small scale expansion is applicable requires an inherently non-perturbative technique. Such an approach that enables us to solve the theory in the non-perturbative domain starting from the underlying QCD Lagrangian is lattice QCD, a discretized version of QCD formulated in terms of Feynman’s path integrals on a space-time lattice preserving gauge symmetry [41]. Like the continuum theory, the only parameters are the bare quark masses and the coupling constant. One recovers continuum physics by extrapolating results obtained at finite lattice spacing  $a$  to  $a = 0$ .

A crucial step, that enables one to numerically evaluate the path integrals needed, is rotation to imaginary

time,  $t \rightarrow -it$ , resulting in the replacement of the time evolution operator  $\exp(-i\mathcal{H}t/\hbar)$  by  $\exp(-\mathcal{H}t/\hbar)$ . Within the Feynman path integral formulation, observables are calculated by a weighted sum over all possible trajectories. In imaginary time it becomes possible to generate a representative ensemble of trajectories by using stochastic methods analogous to those applied in the evaluation of observables in statistical mechanics.

Calculations in lattice QCD started in the early 80’s, and during the first two decades were performed mostly in the quenched approximation, which neglects pair creation. This enormously simplifies the generation of the gauge fields via Monte Carlo methods since one is left with a local gauge action. During the past ten years, theoretical progress in combination with terascale computers have made simulation of the full theory with light pions and large enough volumes feasible using several different discretization schemes. The simplest lattice QCD action is due to Wilson [41]. Nowadays, one uses improved discretized versions of the Dirac operator with reduced finite lattice spacing artifacts and better chiral properties, all of which are expected to yield the same results in the continuum limit [42]. Using these improved fermion discretization schemes, simulations with pion masses within 100 MeV of the physical pion mass are currently available with simulations using improved Wilson fermions even reaching the physical pion mass [43]. A benchmark calculation for lattice QCD is the evaluation of the low lying hadron spectrum, where a systematic study of the hadron masses using different discretization schemes has been performed and the continuum and infinite volume limits have been examined. The agreement with experiment observed from such systematic lattice studies [43, 44], provides a validation of the lattice QCD approach, paving the way to use lattice QCD to provide predictions for quantities, which are very difficult to access experimentally, as for example the e.m. FFs of an excited hadronic state, such as the  $\Delta(1232)$  resonance. It furthermore allows to study how the physics is affected when varying fundamental parameters such as quark masses outside their values realized in nature.

Information on hadron shapes can be extracted from FFs and generalized parton distributions. The evaluation of these quantities is more involved than the computation of hadron masses. FFs are connected to hadron matrix elements of the type  $\langle h'(p') | \mathcal{O} | h(p) \rangle$  and one needs, in general, to compute the diagrams shown in Fig. 9, where the solid lines denote fully dressed quark propagators. The diagram where the operator couples to a sea quark, shown in upper panel of Fig. 9, is particularly difficult to calculate since it involves a disconnected quark loop. For the evaluation of transition FFs where the final hadron state  $h'$  has different quantum numbers from the initial  $h$ , the disconnected diagram vanishes. For diagonal matrix elements, assuming isospin symmetry, the disconnected contribution vanishes for isovector operators and therefore isovector FFs can be calculated from the connected diagram alone. Although recently efforts to cal-

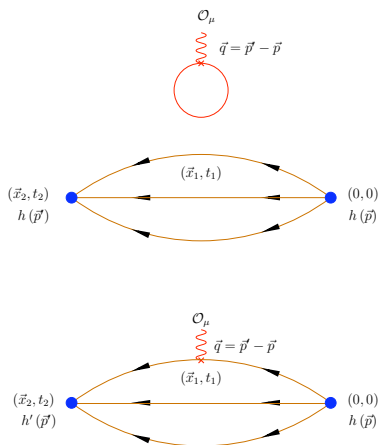


FIG. 9: Upper panel: Disconnected; Lower panel: connected diagrams. With  $h$  and  $h'$  we denote hadronic states and with  $\mathcal{O}$  the operator of interest.

culate such disconnected contributions have intensified, up to now lattice computations of FFs generally neglect disconnected contributions. The standard procedure to evaluate the connected three-point function shown in the lower panel of Fig. 9 is to compute the so called sequential propagator, a convolution of fixed source quark propagators, which are technically straight forward to calculate. In most recent studies of the e.m. FFs the fixed sink method is used. Its name comes from the fact that we consider a given final state  $h'$  is at a *fixed* time  $t_2$  from the initial state  $h$  created at time zero. Within this approach, any operator can be inserted at any intermediate time slice  $t_1$ , as seen in Fig. 9, carrying any possible value of the lattice momentum. For a recent review, which includes comparison of nucleon electromagnetic FFs within a number of different discretization schemes see Ref. [45].

To probe hadron deformation, the e.m. current is used for the operator  $\mathcal{O}$  in Fig. 9. Lower moments of transverse spin densities of quarks in the nucleon [46] or pion [47] as well as the transverse momentum dependent parton distribution functions [45] can also be evaluated using these techniques.

As an example of the predictive power of lattice QCD, we show in Fig. 10 the transverse charge density of Eq. (5) for a  $\Delta^+(1232)$  that has a transverse spin projection  $s_\perp = +3/2$ . This charge density is obtained from the  $\Delta$  e.m. FFs, calculated within lattice QCD in Ref. [48], as described in more detail in Section IV. As can be seen from Fig. 10, the quark charge density in a  $\Delta^+$  in a state of transverse spin projection  $s_\perp = +3/2$  is elongated along the axis of the spin (prolate deformation) when observed from a light-front.

Although lattice QCD provides an *ab initio* calculation of fundamental quantities such as FFs or moments of generalized parton distributions, a careful analysis of statistical and systematic errors must be performed before one can reliably compare to experiment. The systematic errors arise because lattice calculations necessarily are

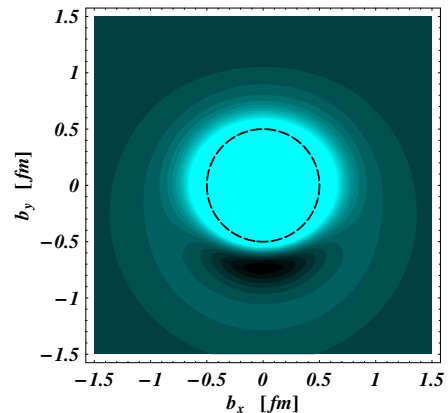


FIG. 10: Lattice QCD results for the quark transverse charge density  $\rho_T^{\Delta^+}_{3/2}$  in a  $\Delta^+(1232)$  which is polarized along the positive  $x$ -axis. The light (dark) regions correspond to the largest (smallest) values of the density. In order to see the deformation more clearly, a circle of radius 0.5 fm is drawn for comparison. The density is obtained from quenched lattice QCD results at  $m_\pi = 410$  MeV for the  $\Delta$  e.m. FFs [48].

performed for a finite lattice size and spacing  $a$  due to the discretization of space-time, which breaks continuous rotational invariance to a discrete one. These systematic errors need to be investigated by repeating the calculation for various volumes and lattice spacings. Except for hadron masses, where both the infinite volume and zero lattice spacing limits are taken, for other quantities like FFs such an analysis has just began. Another source of systematic error is the fact that FFs calculations still utilize dynamical quarks of larger mass than the physical one. Whereas finite  $a$ , lattice size  $L$  and magnitude of the quark masses are amenable to systematic improvements, rotation to Euclidean space selects a set of observables, determined from the properties of the discrete low-lying states, which can be studied within this framework. Nucleon FFs and moments of parton distributions are examples of such observables. Excited states are more difficult to compute since they are exponentially suppressed as compared to the ground state due to the Euclidean time evolution. Techniques have been developed to extract the low lying excited states, however most calculations are still done in quenched QCD and without an analysis of systematic errors, although some recent results on the excited states of the nucleon using two dynamical quarks have been presented. The study of resonances in lattice QCD is a recent activity. One of the reasons is that up to very recently the quark masses that could be simulated were too large to allow decays. Although extraction of the spectral function from lattice correlators is not feasible since the low energy continuum scattering states dominate, there are theoretical techniques to study the width of resonances [49] that make use of the dependence of the energy on the finite lattice length. These techniques, combined with the background field method,

can yield the magnetic and electric quadrupole moments of resonant states [50]. However, to go beyond the calculation of the decay width and the lower moments to the calculation of FFs for resonances such as the  $\Delta$  is still an open theoretical problem.

In Section IV, we will present results showing the state-of-the-art of the lattice calculations for the e.m. FFs of the  $\Delta(1232)$  resonance, as well as for the e.m. FFs describing the  $\gamma^*N \rightarrow \Delta$  transition, and discuss the resulting theoretical predictions for hadron deformation.

### III. EXPERIMENTAL EVIDENCE

The experimental landscape concerning the investigation of the shape of hadrons has been dominated by the quest for resonant quadrupole amplitudes in the  $\gamma^*N \rightarrow \Delta$  transition in the proton. Recently other reactions have been suggested, e.g. the study of the  $\gamma^*N \rightarrow \Delta$  transition in neutrons or in nuclei, and they may become technically feasible in the near future. In addition, it is understood that the detailed and precise understanding of form factors can bring new complementary information on the issue of the shape of hadrons. In addition to the formidable technical difficulties of accessing new reaction channels to the required precision, the theoretical framework to extract the important physical conclusions needs to be further developed.

The experimental investigation of the  $\gamma^*N \rightarrow \Delta$  transition can be classified according to the reaction channel probed. The  $\Delta^+(1232)$  can be excited by real or virtual photons,  $\gamma^*$ , and decays through pion or photon emission:

$$\begin{aligned} \gamma^*p &\rightarrow \Delta^+(1232) \rightarrow p\pi^0 \quad (66\%), \\ \gamma^*p &\rightarrow \Delta^+(1232) \rightarrow n\pi^+ \quad (33\%), \\ \gamma^*p &\rightarrow \Delta^+(1232) \rightarrow p\gamma \quad (0.56\%). \end{aligned}$$

The pion decay channels have been extensively explored while the third, involving the gamma decay branch, has been studied with real compton scattering (RCS). Virtual compton scattering measurements (VCS) are beginning to emerge with the aim of mapping the polarizabilities at high missing mass [51] and/or investigating the issue of deformation [52].

The first generation  $\gamma^*N \rightarrow \Delta$  and in general nucleon resonance experiments were conducted in the late sixties and early seventies, before the issue of deformation was even raised, at DESY, NINA and CEA with low quality beams and experimental equipment not designed to address such refined questions. The data that emerged were characterized by limited accuracy, but they did provide valuable guidance on the design of future experiments [53]. The second generation experiments were obtained by a newer generation of accelerators at Brookhaven, Bates, MAMI, and CEBAF with optimized equipment and in general with polarized beams. Third generation experiments are now beginning to emerge; they have been conducted primarily with polarized and tagged real photons, impinging on polarized

targets. Electroproduction experiments with polarized targets are particularly difficult with only one measurement reported in the literature using the internal target facility at NIKHEF [54] and having low statistical accuracy. The JLab Hall A experiment [55], which presented high quality extensive recoil polarization measurements using polarized beams, is a truly third generation experiment, which both demonstrated the feasibility of the technique, the precision that can be achieved and the rich physics output that can emerge.

In general, in the real photon sector, the “second generation” experiments are completed and analyzed and the era of “third generation” experiments is about to begin in earnest, in view of the important instrumentation initiatives [56] at Mainz and at Bonn. JLab and MAMI C have optimal beams and detection systems for the pursuit of this program, which is far from being exhausted.

The “deformation” signal in the real photon sector comes from the study of the transverse electric quadrupole ( $E_{1+}^{3/2}$  also denoted by E2) multipole. If virtual photons are used, the longitudinal quadrupole ( $L_{1+}^{3/2}$  or C2) is also accessed. The superscript indicates the total isospin 3/2, whereas the subscript denotes the  $l = 1$  angular momentum in the  $\pi N$  system, and the “+” refers to the total angular momentum  $J = l + 1/2 = 3/2$ . In a quark-model picture, the  $\gamma N \rightarrow \Delta$  transition is described by a spin flip of a quark in an  $S$ -wave state in the nucleon, resulting in a magnetic dipole ( $M_{1+}^{3/2}$  or M1) transition. Any  $D$ -wave admixture in the nucleon or the  $\Delta$  wave functions, also allows non-zero values for the electric quadrupole (C2 and E2) transition. This is depicted graphically in Fig. 11.

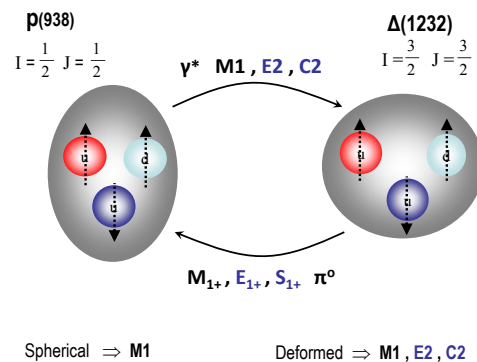


FIG. 11: Quark model picture of  $M1$ ,  $E2$  and  $C2$  amplitudes in the  $N \rightarrow \Delta$  transition induced by the interaction of a photon (real or virtual) with a single quark in the nucleon. Presence of quadrupole amplitudes in the transition requires  $N$  and/or  $\Delta$  wave functions to have a  $D$ -wave component (indicated by a non-spherical shape).

It has become standard practice in the field to measure the resonant quadrupole strengths relatively to the resonant dipole by introducing the ratios  $\text{EMR} = \text{Im}E_{1+}^{3/2}/\text{Im}M_{1+}^{3/2}$  and  $\text{CMR} = \text{Im}L_{1+}^{3/2}/\text{Im}M_{1+}^{3/2}$ .  $\text{EMR}$

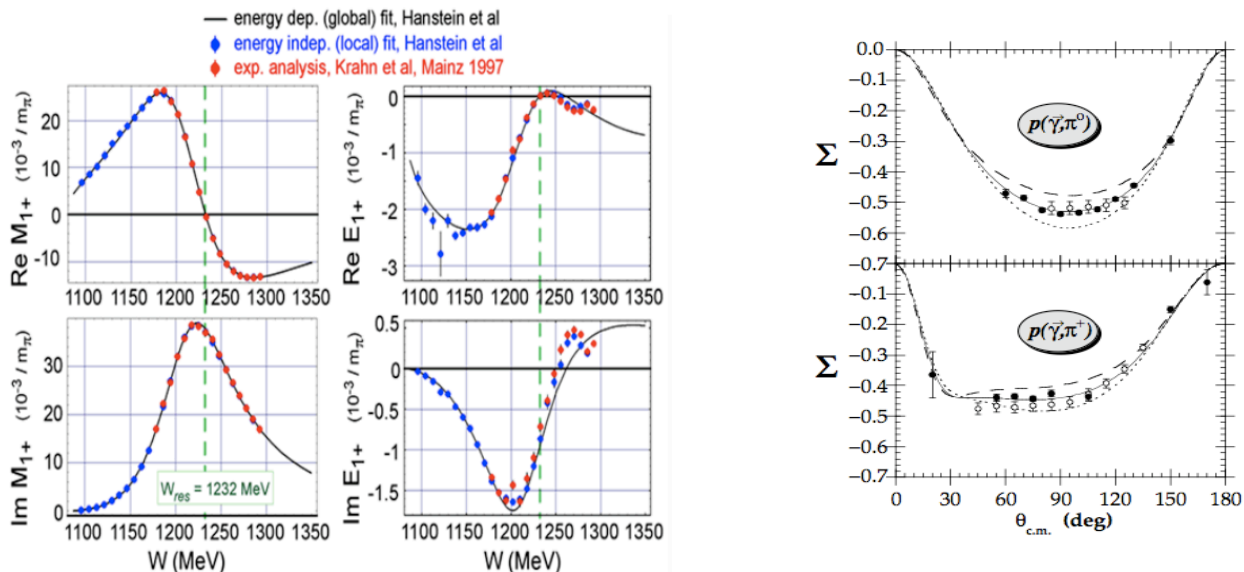


FIG. 12: Results from MAMI (left) and LEGS (right) have yielded precise measurements of the resonant quadrupole amplitude at the photon point. A most sensitive probe is the polarization asymmetry  $\Sigma$  which has been measured precisely at both MAMI and LEGS. The derived multipoles from the MAMI cross sections, yield an accurate measurement of EMR.

and CMR have thus become the signal of deformation.

### A. Real Photon Measurements

In photoproduction, the presence of a resonant quadrupole amplitude, is particularly hard to isolate because the transverse channel is overwhelmed by the magnetic dipole (M1) amplitudes and contaminated with other "background" (non resonant) processes of similar magnitude. In this sense, the  $E_{1+}^{3/2}$  appears in next to leading order (NLO) in photoproduction. Precision measurements with polarized tagged photons performed at Mainz (MAMI) and Brookhaven (LEGS) in the late nineties represent a *tour de force* of experimental finesse. The small quadrupole amplitude has been detected in the measurement of the polarization asymmetry  $\Sigma = (\sigma_{\parallel} - \sigma_{\perp}) / (\sigma_{\parallel} + \sigma_{\perp})$  shown in the right panel of Fig. 12. The asymmetry  $\Sigma$  is measured with reduced systematic error by flipping the polarization of the tagged photon beam parallel ( $\parallel$ ) and perpendicular ( $\perp$ ) to the scattering plane. Analysis of the MAMI  $(\gamma, \pi^+)$  and  $(\gamma, \pi^0)$  data, yields the impressive results shown in the left panel of Fig. 12. It is obvious from this figure that the derived results heavily depend on the  $W$  dependence of the cross section. The  $E_{1+}^{3/2}$  multipoles have a striking non-resonant shape, a manifestation of the complicated processes that contribute to this channel. The measurements from MAMI [57] and LEGS [58] have converged as far as the determination of the asymmetries are concerned. The resulting EMR values are :

$$\begin{aligned} \text{LEGS} &: \text{EMR} = -(3.07 \pm 0.26_{\text{stat.}+\text{sys.}} \pm 0.24_{\text{mod.}})\%, \\ \text{MAMI} &: \text{EMR} = -(2.5 \pm 0.1_{\text{stat.}} \pm 0.2_{\text{sys.}})\%. \end{aligned}$$

A number of theoretical calculations are in good agreement with the experimentally derived EMR value. Both the  $(\gamma, \pi^0)$  and the  $(\gamma, \pi^+)$  channels have been studied extensively. The  $(\gamma, \gamma)$  channel (RCS) has also been studied [59], where the resonance pion-photoproduction amplitudes were evaluated leading to the multipole EMR (340 MeV)  $= (-1.6 \pm 0.4_{(\text{stat}+\text{sys})} \pm 0.2_{(\text{model})})\%$ , in reasonable agreement with the photopion measurements.

The situation concerning the  $\gamma N \rightarrow \Delta$  transition in the real photon sector has remained stable, without experimental results reported to change this picture in the last five years. A subsequent analysis [60] and new data [61] give  $\text{EMR} = (-2.74 \pm 0.03_{(\text{stat})} \pm 0.3_{(\text{sys.})})\%$ , confirming the EMR values of Ref. [57, 58]. In the closely related areas of threshold pion production [62] and in the measurement of the magnetic dipole [33, 63] of the  $\Delta^+(1232)$ , the precise results that emerged provide both a test as well as valuable guidance to theory and phenomenology that is common to both. The installation of the Crystal Ball at MAMI and of the Crystal Barrel at ELSA, have brought new very powerful tools, which are expected to yield even more precise data and results.

### B. Electroproduction measurements

In electron scattering experiments, in addition to the transverse responses, the longitudinal responses are also accessible, which are sensitive to leading order to the longitudinal quadrupole multipole,  $L_{1+}^{3/2}$  or C2. Furthermore, the  $Q^2$  evolution of the various responses offers the ability to distinguish between different processes. This is of particular value for the understanding of the distinctive roles played by the mesonic cloud as compared with

the quark core. These advantages are technically challenging and time consuming to realize due, primarily, to the numerous measurements needed to cover the widest possible range of momentum transfers.

Consistent results have been reported from several groups [55, 64–77] at Bates, ELSA, MAMI and JLab mapping the momentum transfer range from  $Q^2=0.06$  to  $6.0 \text{ GeV}^2$  with high precision in a limited number of observables sensitive to the issue of deformation. However, there are still discrepancies on the extracted EMR and CMR values, which are not directly measurable due to the methodology used in extracting multipoles, an issue discussed in the next section.

Starting from the experimental observables, two methods have been used for extracting multipole amplitudes: a) The Truncated Multipole Expansion (TME) approximation in which most or all of the non-resonant multipoles are neglected (e.g. see [64, 66]) assuming that, at resonance, only the resonant terms contribute significantly and are fitted to the data, and b) the Model Dependent Extraction (MDE) method where a phenomenological reaction framework with adjustable quadrupole amplitudes is used, e.g. see [66, 67, 73]. It is assumed that the reaction is controlled at the level of precision required for the disentanglement of the background from the resonance amplitudes. Clearly the MDE method is superior, given the sophistication that phenomenological models have achieved in describing the data.

In the recent electroproduction experiments, which almost invariably are carried out with polarized beams, the transverse-longitudinal response functions  $\sigma_{TL}$  and  $\sigma_{TL'}$  are measured. Their simultaneous measurement allows the extraction of the real and imaginary parts of the same combination of multipole amplitudes. Knowledge of both responses is particularly valuable because  $\sigma_{TL}$  is most sensitive to the presence of a resonant longitudinal quadrupole amplitude, while  $\sigma_{TL'}$  is particularly sensitive to the background contributions, thus providing information on the two aspects of the problem that need to be controlled independently [78]. The importance of background is clearly seen in the W behavior of the responses [67] and the non-vanishing recoil polarization  $P_n$  [65, 68], which bears close resemblance to  $\sigma_{TL'}$ . The transverse-transverse response,  $\sigma_{TT}$ , which is sensitive to the electric quadrupole amplitude, was only recently isolated for the first time at non-zero  $Q^2$ , with experiments pursued at Bates, JLab and MAMI [79, 80].

Fig. 13 offers a compilation of CMR and EMR as a function of  $Q^2$ . Both EMR and CMR are small and negative in the region where they have been measured. From the accuracy of the present data one immediately recognizes that the quark model predictions, which historically provided the motivation for these measurements, do not agree with the data. In particular the dominant M1 matrix element is found to be  $\simeq 30\%$  stronger and the E2 and C2 amplitudes at least an order of magnitude larger and often of a different sign than the predictions of quark models. This failure is to be expected since the quark

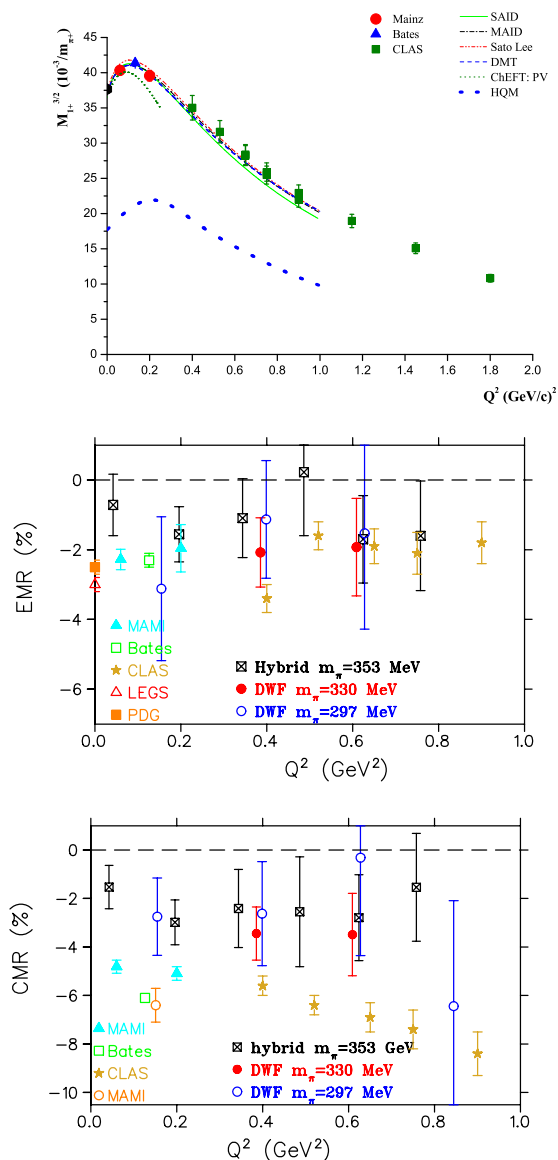


FIG. 13: The experimentally derived values for  $M_{1+}^{3/2}$  (M1) (top panel), CMR (middle panel) and EMR (lower panel) compared to phenomenological model results for M1, and to lattice for EMR and CMR. The derived multipole ratios are shown without the model error that is of the order or larger than the depicted experimental error.

model does not respect chiral symmetry whose dynamic breaking leads to a strong, non-spherical, pion cloud surrounding hadrons [81]. As will be discussed in detail in Section IV, it was realized that the pion cloud was a necessary ingredient to be added to quark models. This is demonstrated by the calculations of the SL [39] and DMT [40] models, which describe the data adequately, and which show that most of the strength of the re-

sponses (and the EMR and CMR values) at very low  $Q^2$  values, below  $\simeq 0.25 \text{ GeV}^2/c^2$ , arises on account of the mesonic degrees of freedom. The recent results from MAMI along with the earlier ones from Bates [79] and the recent low  $Q^2$  measurements from CLAS [80], give strong support to this interpretation. At asymptotic values of  $Q^2$  helicity conservation [82] requires that  $\text{EMR} \rightarrow 1$  and that  $\text{CMR} \rightarrow \text{constant}$ . Clearly this regime has not been reached. The upgrade of CEBAF to 12 GeV will allow to extend the measurements to higher  $Q^2$ , although this will pose significant challenges in isolating the relevant partial cross sections and even bigger ones in extracting the relevant amplitudes.

Finally, the  $H(\vec{e}, e'p) \gamma$  channel (VCS), which only recently has been accessed, allows the extraction of the quadrupole amplitudes through a purely electromagnetic reaction channel providing an important cross check to the derived results from the pionic channel. The dispersion theory of Ref. [83], allows one to address the physics of deformation and of nucleon polarizabilities in the region above pion threshold simultaneously. Recent results from MAMI report the extraction of polarizabilities [51] and the first observation of VCS data sensitive to the resonant quadrupole amplitudes [52]. The results are in excellent agreement with those derived from the pion channel.

### C. Sensitivity, Precision and Estimation of Uncertainties

The  $\gamma^*N \rightarrow \Delta$  data up to  $Q^2 = 6.0 \text{ GeV}^2$  are, in general, characterized by small systematic errors and high statistical precision. The interpretation of the data in terms of the deformation has been demonstrated, and as a result, the research thrust shifted from the investigation of whether the conjecture for deformation is valid to the exploration of the mechanisms that cause it. Investigating the physical origin of deformation requires the measurement of new responses and the comparison of the theoretical results with the experimentally derived quantities, at a level of precision far superior to the one feasible today. This detailed comparison necessitates a reliable determination of the uncertainties of both the experimental results and the theoretical calculations.

The need for a critical and precise comparison of data and theory when extracting multipoles in nucleon resonance studies is reminiscent of the “crisis” in the analysis of electron scattering data in the early 1970s, where the very precise data could not be meaningfully compared with the theoretical calculations in order to derive nuclear charge densities. This was primarily due to the lack of an appropriate methodology that could enable to quantify the uncertainties in the extracted densities, which, like multipole amplitudes, are not experimental observables. The resolution of the “crisis” through the introduction of a “Model Independent” extraction of charge densities led to a revolution in the field and to the

outstanding achievements in electron scattering.

The leading method of extraction of multipole amplitudes, the Model Dependent Extraction (MDE), produces extracted values that are biased by the model and characterized by a model error, which is hard to estimate, especially if a single model is employed [66, 68, 70, 72, 74]. An *Ansatz* for estimating the model uncertainties in the extracted multipoles has been proposed [84, 85] and used in a few cases [71, 73]. In this method the same data are analyzed employing different models, which describe the data adequately, and attributing the resulting spread in the extracted quantities to model uncertainty. Even though the phenomenological models available are of considerable sophistication, the small non-resonant amplitudes collectively could induce large correlations and error in the extraction of the resonant amplitudes, resulting in the unsatisfactory situation that the uncertainty is only approximately known.

A novel model independent method, the Athens Model Independent Analysis Scheme (AMIAS), for extracting multipole information from experimental nucleon resonance [86] and for analyzing lattice QCD simulation data has been presented [87]. The method quantifies the uncertainty of the extracted multipoles and yields new information on background amplitudes, which MDE is incapable of accessing [85]. Results from AMIAS are shown in Fig. 8 (yellow bands) for the CMR sensitive  $\sigma_{LT}$  partial cross section with the precisely defined one- $\sigma$  uncertainty. The experimentally allowed  $\sigma_{LT}$  partial cross section, as constrained by the Bates and MAMI data at  $Q^2 = 0.127 \text{ GeV}^2$ , are shown as a function of  $\theta_{pq}^*$ . They are compared with theoretical model predictions that account for them. It is evident that the model predictions (dotted curves) with resonant quadrupole amplitudes set to zero, which amounts to spherical solutions, are excluded with high confidence. On the contrary model predictions from models that allow mesonic degrees of freedom allowing for deformation are in reasonable agreement with the experimental results at the  $2\sigma$  level. Differences among the curves predicted by the various phenomenological models are visible, but no inference can be drawn as their model error is not known. *Nevertheless, the comparison demonstrates with extremely high confidence, with experimental errors precisely defined, that the assumption of sphericity for both the nucleon and the  $\Delta^+(1232)$  is incompatible with the data.*

## IV. THE SHAPE OF NUCLEON AND $\Delta$ RESONANCE : THEORETICAL UNDERSTANDING

Having seen first experimental evidence for a non-spherical shape of the nucleon and  $\Delta$  resonance, we next discuss its theoretical understanding. For the  $\Delta$  resonance, its e.m. FFs are not accessible experimentally. They are, therefore, an ideal example of observables where lattice QCD can make predictions. The state-of-

the-art of these calculations as well as their implication on the shape of the  $\Delta$  resonance are discussed. Subsequently our current theoretical understanding of the  $\gamma^*N \rightarrow \Delta$  transition is summarised including an interpretation of the data presented in Section III.

### A. $\Delta$ charge densities : lattice QCD

As the nucleon is a spin-1/2 particle, its transverse charge densities do not exhibit a quadrupole pattern, nor do they encode any information on its shape. For spin-3/2 baryons, such information can however be obtained from the charge densities.

The matrix element of the e.m. current operator  $J^\mu$  between spin-3/2 states, such as the  $\Delta(1232)$  resonance, can be decomposed into four multipole transitions: Coulomb monopole (E0), magnetic dipole (M1), Coulomb quadrupole (E2) and magnetic octupole (M3), described by the corresponding FFs  $G_{E0}$ ,  $G_{M1}$ ,  $G_{E2}$  and  $G_{M3}$  [88, 89]. Their values at  $Q^2 = 0$  define e.g. the magnetic dipole moment :  $\mu_\Delta = G_{M1}(0)e/(2M_\Delta)$ , or the electric quadrupole moment :  $Q_\Delta = G_{E2}(0)e/M_\Delta^2$ .

The empirical knowledge of the  $\Delta$  electromagnetic moments is scarce, even though there were several attempts to measure its magnetic dipole moment. The current PDG value of the  $\Delta^+$  magnetic dipole moment is [30]:

$$\mu_{\Delta^+} = 2.7_{-1.3}^{+1.0}(\text{stat.}) \pm 1.5(\text{syst.}) \pm 3(\text{theor.}) \mu_N. \quad (13)$$

This result was obtained from *radiative photoproduction* ( $\gamma N \rightarrow \pi N \gamma'$ ) of neutral pions in the  $\Delta(1232)$  region by the TAPS Collaboration at MAMI [63], using a phenomenological model of the  $\gamma p \rightarrow \pi^0 p \gamma'$  reaction. For the  $\Delta^+$ , Eq. (13) implies :

$$G_{M1}(0) = 3.5_{-1.7}^{+1.3}(\text{stat.}) \pm 2.0(\text{syst.}) \pm 3.9(\text{theor.}). \quad (14)$$

The size of the error-bar is rather large due to both experimental and theoretical uncertainties.

For the  $\Delta$  electric quadrupole moment or magnetic octupole moments, no direct measurements exist, nor do we have any empirical information on the  $Q^2$  behavior of the  $\Delta$  e.m. FFs. We thus rely on recent lattice QCD calculations [48] that can predict these FFs.

Calculation of the e.m. FFs within lattice QCD requires the evaluation of a three-point function, as depicted in Fig. 9. We only consider here the connected diagram. Its evaluation involves two spatial sums : one over the spatial coordinates of the operator and one over the spatial coordinates of the final state. In the so-called fixed sink method, the sum over  $\vec{x}_2$  is done automatically by generating a sequential (backward) propagator from the sink to the operator. Inserting the operator, which can be done at all values of  $\vec{x}_1$ , and summing over  $\vec{x}_1$  with the appropriate Fourier phase and propagator starting at  $t = 0$  and ending at  $t = t_1$  yields the connected three-point function, for all momentum transfers  $\vec{q}$ . To extract the matrix element  $\langle h'(p') | \mathcal{O} | h(p) \rangle$  one studies the large

$t_1$  Euclidean time behavior of an appropriately defined ratio of the three-point function and two-point functions, yielding a time independent quantity (plateau). Such a behavior signals identification of the lowest hadron states  $h$  and  $h'$  from the tower of QCD states with the same quantum numbers as  $h$  and  $h'$ . Fitting to this plateau value we extract the matrix element  $\langle h'(p') | \mathcal{O} | h(p) \rangle$  and from this, depending on the choice of  $\mathcal{O}$ , the FFs or moments of parton distributions.

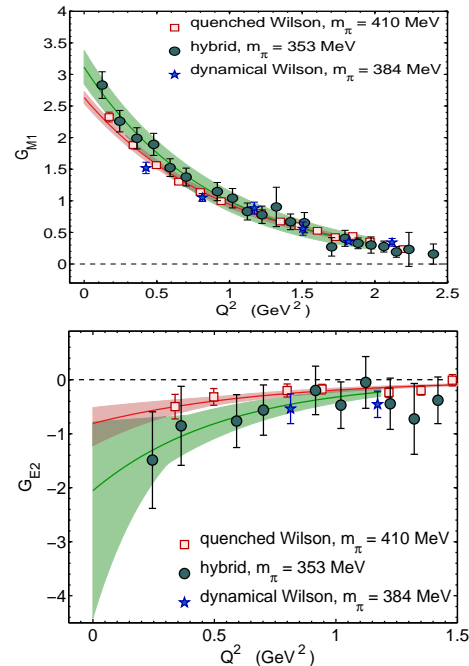


FIG. 14: Lattice results for the  $\Delta^+(1232)$  form factor  $G_{M1}$  (upper panel) and  $G_{E2}$  (lower panel) at the smallest pion mass in three simulations [48]. The lines show the fits to an exponential form of the quenched lattice results and to the results obtained using the hybrid action. The error band is calculated using a jackknife analysis on the fitted parameters.

To probe hadron deformation we will use in the following the e.m. current as the operator  $\mathcal{O}$ . Since the connected diagram for the  $\Delta$  e.m. FFs is calculated by performing sequential inversions through the sink, the initial and final  $\Delta$  states need to be fixed. The  $\Delta$  is described by a Rarita-Schwinger spinor and therefore there is some freedom in the vector indices that can be chosen. Ref. [48] concentrates on a few carefully chosen combinations that best determine the three FFs paying particular attention in constructing a combination that isolates the electric quadrupole FF. In order to efficiently check the lattice set-up, a quenched calculation is carried out using Wilson fermions and the standard Wilson plaquette gauge action [48] for which statistical fluctuations are small. Quenched results are then compared to a calculation using two dynamical degenerate flavors of Wilson fermions ( $N_F = 2$ ) and the standard Wilson plaquette gauge-action as well as using a hybrid action [48]. The latter case uses two degenerate flavors

of light staggered sea quarks and a strange staggered sea quark ( $N_F = 2 + 1$ ) simulated using the Asqtad MILC action [90]. The strange quark mass is fixed to its physical value. These gauge configurations are among the best simulations of the QCD vacuum available. The valence quarks are domain wall fermions (DWF) that preserve a form of chiral symmetry on the lattice. A comparison between results obtained with these two different lattice formulations for the quarks (i.e. dynamical Wilson and staggered sea with DWF) provides a non-trivial check of lattice artifacts. In both dynamical simulations the  $\Delta$  is a stable particle.

We show the results for the  $\Delta$  FFs  $G_{M1}$  and  $G_{E2}$  in Fig. 14. For the pion masses considered, there is agreement among results using the different actions, with statistical errors being smallest in the quenched theory, as expected. For the  $\Delta$  magnetic dipole moment, first dynamical results, using a background field method, with  $N_F = 2 + 1$  quark flavors were presented in Ref. [50]. The magnetic moment can also be extracted by fitting the  $Q^2$ -dependence of the magnetic dipole form factor  $G_{M1}$  to determine its value at  $Q^2 = 0$ . The values obtained in these two approaches are in agreement [48].

Having a determination of the  $\Delta$  e.m. FFs in lattice QCD one can calculate its transverse light-front charge density  $\rho_T^\Delta|_{s_\perp}$  [48], as shown in Fig. 10. Choosing the transverse spin vector  $\vec{S}_\perp = \hat{e}_x$ , the electric quadrupole moment in a state of  $s_\perp = +3/2$  for such charge distribution is then obtained from Eq. (6) as :

$$Q_{+\frac{3}{2}} = \frac{1}{2} [2(G_{M1}(0) - 3e_\Delta) + (G_{E2}(0) + 3e_\Delta)] \left( \frac{e}{M_\Delta^2} \right). \quad (15)$$

Note that for a spin-3/2 particle without internal structure, for which  $G_{M1}(0) = 3e_\Delta$  and  $G_{E2}(0) = -3e_\Delta$ , the quadrupole moment of its transverse light-front charge density vanishes. This is in contrast with the non-relativistic case, where a non-zero value of  $G_{E2}$  is usually interpreted as a non-zero quadrupole moment in the lab frame. It is thus interesting to observe from Eq. (15) that, as for the case of a spin-1 particle discussed in Section II,  $Q_{s_\perp}$  is only sensitive to the anomalous parts of the spin-3/2 magnetic dipole and electric quadrupole moments, and vanishes for a particle without internal structure. Extrapolating the  $\Delta$  e.m. FFs to  $Q^2 = 0$ , and using the extracted values in Eq. (15) yields a quadrupole moment  $Q_{+\frac{3}{2}}$ , of  $(0.73 \pm 0.16) (e/M_\Delta^2)$  for the quenched and  $(0.51 \pm 0.22) (e/M_\Delta^2)$  for the hybrid cases. Both calculations therefore show a (small) prolate deformation of the two-dimensional light-front charge density along the axis of the  $\Delta$  spin (for the case of spin projection  $+3/2$ ).

## B. The electromagnetic $N \rightarrow \Delta$ transition in QCD

### 1. Electromagnetic moments and densities

Direct experimental evidence for a deformation of  $N$  and  $\Delta$  states can be obtained from the  $\gamma^* N \Delta$  transition, which is usually characterized in terms of three Jones–Scadron FFs [91] :  $G_{M1}^*$ ,  $G_{E2}^*$  and  $G_{C2}^*$ , denoting the magnetic dipole, electric quadrupole and Coulomb quadrupole transitions respectively. For a review and more details see Ref. [89]. In the following, we will often discuss the ratios EMR and CMR, which are expressed in terms of the Jones-Scadron FFs as:

$$\text{EMR} = -\frac{G_{E2}^*}{G_{M1}^*}, \quad \text{CMR} = -\frac{Q_+ Q_-}{4M_\Delta^2} \frac{G_{C2}^*}{G_{M1}^*}, \quad (16)$$

with  $Q_\pm \equiv \sqrt{(M_\Delta \pm M_N)^2 + Q^2}$ .

From the experimental information on the  $\gamma^* N \Delta$  transition, discussed in Section III, one can extract the transition magnetic dipole and electric quadrupole moments from the values of the FFs at  $Q^2 = 0$  [92]:

$$\mu_{N \rightarrow \Delta} = \sqrt{M_\Delta/M_N} G_{M1}^*(0) [\mu_N], \quad (17)$$

$$Q_{N \rightarrow \Delta} = -6\sqrt{M_\Delta/M_N} \frac{2M_\Delta}{M_N(M_\Delta^2 - M_N^2)} G_{E2}^*(0) \quad (18)$$

Using the experimental information, this yields [92] :

$$\mu_{p \rightarrow \Delta^+} = [3.46 \pm 0.03] \mu_N, \quad (19)$$

$$Q_{p \rightarrow \Delta^+} = -(0.0846 \pm 0.0033) \text{ fm}^2. \quad (20)$$

One often uses an equivalent parametrization for the  $\gamma N \Delta$  transition at the real photon point ( $Q^2 = 0$ ) through two helicity amplitudes  $A_{1/2}$  and  $A_{3/2}$ , where the subscript denotes the total  $\gamma + N$  helicity in the  $\Delta$  rest frame. Furthermore, one can generalize the considerations for the nucleon and  $\Delta$  FFs to extract from the empirical information on the  $Q^2$  dependence of the  $M1$ ,  $E2$ , and  $C2$  transition FFs, the quark transition charge densities in the transverse plane, which induce the e.m.  $N \rightarrow \Delta$  excitation [23]. The transition density in a transversely polarized  $N$  and  $\Delta$  shows both monopole, dipole, and quadrupole patterns. The latter, shown in Fig. 15, maps the spatial dependence in the deformation of the transition charge distribution.

### 2. Model descriptions of the $\gamma^* N \Delta$ transition

As discussed above, the e.m.  $N \rightarrow \Delta$  transition is predominantly of the magnetic dipole ( $M1$ ) type. A first understanding of the  $\gamma^* N \Delta$  transition can be obtained based on symmetries of QCD and its large number-of-color ( $N_c$ ) limit. In this limit, the baryon sector composed of up, down, and strange quark flavors of QCD displays an  $SU(6)$  spin-flavor symmetry. This spin-flavor global symmetry of QCD is at the basis of



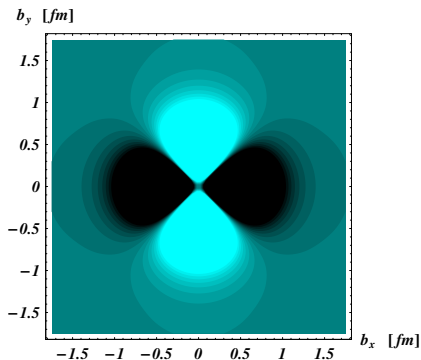


FIG. 15: Quadrupole contribution to the transverse charge density for the  $p \rightarrow \Delta^+$  transition, when  $N$  and  $\Delta$  are polarized along the  $x$ -axis with spin projection  $+1/2$ . For the  $N \rightarrow \Delta$  e.m. FFs, the phenomenological MAID2007 [38] parametrization is used. Figure from Ref. [23].

many quark models, in which baryons are described as (non-relativistic) quantum-mechanical three-quark systems moving in a confining potential. In such quark-model picture, the  $N \rightarrow \Delta$  transition is described by an  $M1$  spin flip of a quark in the  $S$ -wave state, illustrated in Fig. 11. The  $SU(6)$  symmetry allows to relate the magnetic dipole moments of the proton and the  $p \rightarrow \Delta^+$  transition as :  $\mu_{p \rightarrow \Delta^+} = 2\sqrt{2}/3 \mu_p = 2.63 \mu_N$ , which is about 25 % lower than the experimental number of Eq. (19). Any  $D$ -wave admixture in the nucleon or the  $\Delta$  wave functions allows non-zero values for the  $E2$  and  $C2$  quadrupole transitions, as illustrated in Fig. 11.

The prototype quark model is the Isgur-Karl model [93], where the constituent quarks move in a harmonic oscillator type long-range confining potential, which is supplemented by an interquark force corresponding with one-gluon exchange. The one-gluon exchange leads to a color hyperfine interaction, which was found to predict well the mass splittings between octet and decuplet baryons [94]. This hyperfine interaction contains a tensor force which produces a  $D$ -state admixture in the  $N$  and  $\Delta$  ground states, around 1 % [15, 95]. As a result of such  $D$ -wave components, the  $N$  and  $\Delta$  charge densities become non-spherical, yielding small negative EMR values, in the range  $-0.8\% < \text{EMR} < -0.3\%$  within non-relativistic quark models [15, 96]. The small value for EMR already indicates that any effect of deformation in the nucleon and/or  $\Delta$  ground state is rather small and very sensitive to details of the wave function, as well as truncation in the quark model basis [97, 98]. The error induced due to the truncation in the quark model basis has been further investigated in the relativized quark model [99], typically resulting in an even smaller negative value, namely  $\text{EMR} \simeq -0.2\%$ .

Even though the constituent quark model, despite its simplicity, is relatively successful in predicting the structure and spectrum of low-lying baryons, it under-predicts  $\mu_{N \rightarrow \Delta}$  by more than 25 % and leads to values for EMR, which are typically smaller than experiment. More gen-

erally, constituent quark models do not satisfy the symmetry properties of the QCD Lagrangian. In the limit of massless up and down (current) quarks, the QCD Lagrangian is invariant under  $SU(2)_L \times SU(2)_R$  rotations of left ( $L$ ) and right ( $R$ ) handed quarks in flavor space. This *chiral symmetry* is spontaneously broken in nature leading to the appearance of massless Goldstone modes, pions, which acquire a mass due to the explicit breaking of chiral symmetry. Since pions are the lightest hadrons, they dominate the long-distance behavior of hadron wave functions. As the  $\Delta(1232)$  resonance nearly entirely decays into  $\pi N$ , the pions are of particular relevance to the  $\gamma^* N \Delta$  transition. Therefore, a natural way to qualitatively improve on the above-mentioned constituent quark models is to include the pionic degrees of freedom.

Early investigations of the  $\gamma^* N \Delta$  transition including pionic effects were performed within the *chiral bag model* [100, 101], which was developed as an improvement to the MIT bag model [102] by introducing an elementary pion, which couples to quarks in the bag in such a way that chiral symmetry is restored [103]. Calculations within the chiral bag model [104], found that with a bag radius,  $R$ , around 0.8 fm one is able to obtain a reasonably good description for the helicity amplitudes, as can be seen from the values given in Table I. For such a small bag radius, the pionic effects are crucial as they account for around 75 % of the total strength of the amplitude  $A_{3/2}$ . The same calculation however yields  $\text{EMR} \simeq -0.03\%$ , in disagreement with experiment.

The role of the pion-cloud contributions is also highlighted in *Skyrme models* [105, 106], in which the nucleon appears as a soliton solution of an effective non-linear meson field theory. The inclusion of rotational corrections in such models, leads to a quadrupole distortion of the classical soliton solution, yielding a value for  $\text{EMR} = -2.3\%$  [106], consistent with experiment.

The EMR ratio has also been calculated in models, with both quarks and pion degrees of freedom such as the *chiral quark soliton model* ( $\chi$ QSM), which interpolates between a constituent quark model and the Skyrme model [107]. For the two flavor case, one finds  $\text{EMR} = -2.1\%$  [108], fairly close to experiment, considering that in the  $\chi$ QSM calculation no parametrization adjustment has been made to the  $N \rightarrow \Delta$  transition. However, the magnitudes of the photocouplings, which are given in Table I, are largely under-predicted in the  $\chi$ QSM.

A number of subsequent works have revisited quark models, restoring chiral symmetry by including two-body exchange currents between the quarks. These exchange currents lead to non-vanishing  $\gamma^* N \Delta$  quadrupole amplitudes [109], even if the quark wave functions have no  $D$ -state admixture. Such a picture [109], in which the  $\Delta$  is excited by flipping the spins of two quarks, yields  $\text{EMR} \simeq -3.5\%$ , and relates the  $N \rightarrow \Delta$  and  $\Delta^+$  quadrupole moments to the neutron charge radius as :

$$Q_{p \rightarrow \Delta^+} = r_n^2 / \sqrt{2}, \quad Q_{\Delta^+} = r_n^2. \quad (21)$$

Using the experimental neutron charge radius,  $r_n^2 =$

$-0.113(3) \text{ fm}^2$ , Eq. (21) yields :  $Q_{p \rightarrow \Delta^+} = -0.08 \text{ fm}^2$ , and  $Q_{\Delta^+} = -0.113 \text{ fm}^2$ . This value of  $Q_{p \rightarrow \Delta^+}$  is close to the empirical determination, given in Eq. (20). In such hybrid (quark/pion-cloud) models [110], the pion cloud is fully responsible for the non-zero values of the intrinsic quadrupole moments and hence for the non-spherical shape of these particles. As a summary, we list in Table I the  $\gamma N \Delta$  photo-couplings  $A_{1/2}$  and  $A_{3/2}$  as well as the ratio EMR in various models.

	$A_{1/2}$ [ $10^{-3}$ GeV $^{-1/2}$ ]	$A_{3/2}$ [ $10^{-3}$ GeV $^{-1/2}$ ]	EMR [%]
experiment Ref. [30]	$-135 \pm 6$	$-250 \pm 8$	$-2.5 \pm 0.5$
SU(6) symmetry	-107	-185	0
quark models non-rel. [15, 95–97]	-103	-179	-2 to 0
relativized [99]	-108	-186	-0.2
bag models MIT [102]	-102	-176	0
chiral bag [101]	-106	-198	-1.8
chiral bag [104]	-134	-233	-0.03
Skyrme models [105]			
[106]	-136	-259	-2.3
chiral quarks soliton [108]	-70.5	-133	-2.1
$\pi, \sigma$ exchange [109]	-91	-182	-3.5
[110]	-124.3	-244.7	-3.1

TABLE I: Summary of the  $\gamma N \Delta$  photo-couplings  $A_{1/2}$ ,  $A_{3/2}$ , and EMR in different models compared with experiment.

### 3. Large $N_c$ predictions

Although the results obtained from the different QCD inspired models reviewed above may provide us with physical insight on the  $\gamma^* N \Delta$  transition and its relation to the nucleon and  $\Delta$  shape, they are not a rigorous consequence of QCD. In the following subsections, we will discuss what is known on the  $\gamma^* N \Delta$  transition from approaches, which are directly related with QCD in some limit, such as the  $1/N_c$  expansion of QCD (limit of large number of colors), chiral effective field theory (chiral limit of small pion masses or momentum transfers) or lattice QCD simulations (continuum limit).

The  $1/N_c$  expansion of QCD [111, 112] provides an expansion with a perturbative parameter at all energy scales. This expansion has proved quite useful in describing properties of baryons, such as, ground-state and excited masses, magnetic moments, and electromagnetic decays. For reviews see Refs. [113, 114]. For example, the  $N \rightarrow \Delta$  transition magnetic moment  $\mu_{N \rightarrow \Delta}$  is re-

lated to the isovector nucleon magnetic moment as [115]:  $\mu_{p \rightarrow \Delta^+} = (\mu_p - \mu_n)/\sqrt{2} \simeq 3.23 \mu_N$ , within 10 % of the experimental value of Eq. (19). The EMR value was shown to be of order  $1/N_c^2$  [116]. Thus its smallness is naturally explained in the large  $N_c$  limit.

The large  $N_c$  limit also allows one to relate the  $\Delta$  and  $N \rightarrow \Delta$  quadrupole moments via [117]:  $Q_{\Delta^+}/Q_{p \rightarrow \Delta^+} = 2\sqrt{2}/5 + \mathcal{O}(1/N_c^2)$ , Using the phenomenological value of Eq. (20) yields :  $Q_{\Delta^+} = -(0.048 \pm 0.002) \text{ fm}^2$ , which implies  $G_{E2}(0) = -1.87 \pm 0.08$ .

The relation of Eq. (21) between  $Q_{p \rightarrow \Delta^+}$  and  $r_n^2$  was also shown [117] to hold in the large  $N_c$  limit. Furthermore, it was shown [118] that in the large  $N_c$  limit :

$$\text{EMR} = \text{CMR} = (1/12) R_{N\Delta}^{3/2} (M_\Delta^2 - M_N^2) r_n^2 / \kappa_V, \quad (22)$$

with  $R_{N\Delta} \equiv M_N/M_\Delta$ , and  $\kappa_V = \kappa_p - \kappa_n$ , the isovector nucleon anomalous magnetic moment. Numerically, Eq. (22) yields  $\text{EMR} = \text{CMR} = -2.77\%$ . For EMR this prediction is in an excellent agreement with experiment, Eq. (20). For CMR, where a direct measurement at the real-photon point is not possible, extending the large- $N_c$  relation to finite  $Q^2$  allows relations with the neutron electric FF, which agree well with experiment [118, 119].

### 4. Lattice QCD and chiral effective field theory

Lattice QCD provides the possibility of calculating the  $N$  to  $\Delta$  e.m. FFs starting from the underlying theory of QCD. The set-up for the lattice calculation of the three transition FFs is the same as that used for the extraction of the  $\Delta$  FFs. The advantage in this case is that the connected diagram yields the full contribution. It is calculated by sequential inversion through the sink for the same three simulations as described in the case of the  $\Delta$  FFs. In addition, recent calculations using  $N_F = 2 + 1$  dynamical DWF generated by the RBC and UKQCD collaborations [120] provide a unitary setup and a further check of the results [121]. In all these calculations the pion mass is such that the  $\Delta$  is still stable. Fig. 16 shows a comparison of the lattice results for  $G_{M1}^*$  at the lightest pion mass in each type of simulation. There is agreement among Wilson fermions and results obtained using the hybrid action as well as dynamical DWF. The agreement of results using dynamical fermions with the quenched results indicate that pion cloud contributions due to pair creation are still small at a pion mass of about 330 MeV. As also seen for the nucleon e.m. FFs, lattice results underestimate  $G_{M1}^*$ . Chiral dynamics is expected to induce large corrections at small  $Q^2$  and such effects can be investigated as lattice simulations at smaller pion masses become available.

The CMR and EMR are shown in Fig. 13, and have larger statistical errors due to the fact that  $G_{E2}^*$  and  $G_{C2}^*$ , being sub-dominant, are harder to determine. We show quenched results that have the smallest errors as well as results obtained in the hybrid action approach and using

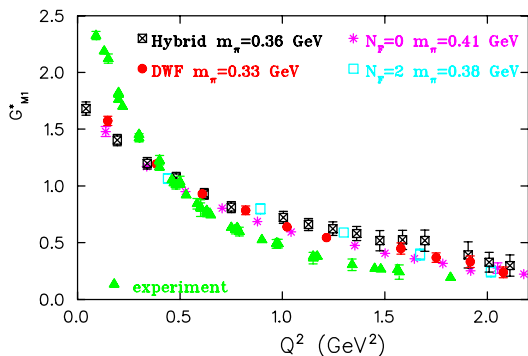


FIG. 16:  $Q^2$ -dependence of the  $N \rightarrow \Delta$  FF  $G_{M1}^*$ , at the lightest pion mass for each type of simulation. Quenched results are shown with the asterisks, results with  $N_F = 2$  Wilson with the open squares, results using the hybrid action with the dotted squares and using DWF with the filled circles. Experimental data from Refs. [57, 67, 70, 73, 75, 122] are shown [v ]}.

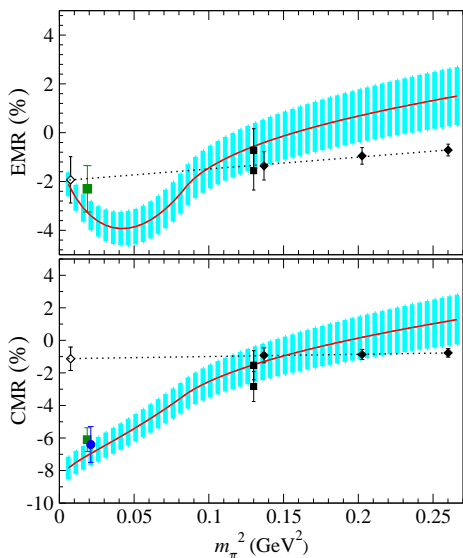


FIG. 17: The  $m_\pi$  dependence of EMR (upper panel) and CMR (lower panel), at  $Q^2 = 0.1 \text{ GeV}^2$ . The data points are from MAMI [68] (blue circle), and BATES [67, 71] (green squares). The filled black diamonds are quenched lattice results [132]. The open diamond near  $m_\pi \simeq 0$  represents their extrapolation assuming linear dependence in  $m_\pi^2$ . The solid black squares at  $m_\pi = 0.36 \text{ GeV}$  are hybrid lattice results [123] at  $Q^2 \simeq 0.04 \text{ GeV}^2$  (upper points) and at  $Q^2 \simeq 0.2 \text{ GeV}^2$  (lower points). The solid red curves are a  $\chi$ EFT result [131]. The (blue) error bands represent the estimate of theoretical uncertainty for the  $\chi$ EFT calculation.

$N_F = 2 + 1$  DWF [121]. The conclusion that can be drawn is that agreement of lattice results on EMR and CMR with experiment is better as compared to that of  $G_{M1}^*$ . Such an agreement is seen also in other ratios, indicating that they are less affected by lattice artifacts than each of the quantities separately.

The present lattice QCD calculations are performed

for quark masses larger than their values in nature. To extrapolate to the physical pion mass, one can use the  $\chi$ EFT of QCD [124–126].  $\chi$ EFT provides a firm theoretical framework at low scales, with the relevant symmetries of QCD built in consistently. The  $\gamma^* N \Delta$  transition provides new challenges for  $\chi$ EFT as it involves the interplay of two light mass scales: the pion mass and the  $N - \Delta$  mass difference. A first study, taking into account these two mass scales, was performed within the framework of heavy-baryon chiral perturbation theory [127]. A more comprehensive study was subsequently carried out [128, 129] using the “ $\epsilon$ -expansion” scheme. In that scheme, the two light scales in the problem: the pion mass  $\epsilon \equiv m_\pi/\Lambda_{\chi\text{SB}}$ , with  $\Lambda_{\chi\text{SB}} \sim 1 \text{ GeV}$  the chiral symmetry breaking scale, and the  $\Delta$ -resonance excitation energy  $\delta \equiv (M_\Delta - M_N)/\Lambda_{\chi\text{SB}}$  are counted as being of the same order, i.e.  $\epsilon \sim \delta$ . To allow for an energy-dependent power-counting scheme designed to take account of the large variation of the  $\Delta$ -resonance contributions with energy, the “ $\delta$ -expansion” scheme has been introduced [130]. It treats the two light scales  $\epsilon$  and  $\delta$  on a different footing, counting  $\epsilon \sim \delta^2$ , the closest integer-power relation between these parameters in the real world. It has been applied to the study of the  $\gamma^* N \Delta$  FFs [131], and has been used in extrapolating the present lattice QCD calculations to the physical pion mass. This is shown in Fig. 17 for the EMR and CMR ratios, which shows that  $\chi$ EFT predicts strong non-analytic dependencies on the quark mass for  $m_\pi < (M_\Delta - M_N)$ , invalidating simple linear extrapolation in  $m_\pi^2$ . In particular, the  $\chi$ EFT results reconcile the lattice results and the relatively large negative experimental value for CMR.

For smaller pion masses, where the  $\Delta$  becomes an open channel, the lattice results will be able to provide momentum-dependent phase-shifts [49]. To extract resonance quantities from those will require a fitting procedure, e.g. Breit-Wigner or complex pole fits, as done when extracting them from experimental multipoles.

## V. CONCLUSIONS

In this review, we have presented the experimental results and theoretical understanding on the shape of hadrons. Although shapes of nuclei have been explored over many decades, it is only in recent years that it became possible to define this question in a theoretically rigorous way for hadrons, and perform the experiments to answer it. The key concept is to quantify size and shape of an extended object through a quantum mechanical density operator. For a relativistic bound state system of near massless quarks, a probability interpretation is obtained by considering the system in a light-front frame, and projecting its charge density along the line-of-sight. We have argued that the resulting transverse charge density encodes the information on hadron size and shape.

On the experimental side, the most accessible and best studied reaction to reveal hadron deformation is the

$N \rightarrow \Delta$  transition. We have reviewed the state-of-the-art experimental techniques, which have allowed to accurately determine the  $N \rightarrow \Delta$  quadrupole amplitudes at low momentum transfers, and establish a deformation in the  $N/\Delta$  system. The quadrupole transitions were pinned down on the order of a few % of the dominant magnetic dipole transition. A quantitative understanding of the small, non-zero values of these amplitudes from the underlying theory, QCD, is a particular challenge. We have provided the historical perspective in which this question was addressed from QCD inspired models, highlighting the role the pions play in these transitions. It is only very recently, however, that *ab initio* calculations became possible, and state-of-the-art full lattice QCD simulations for both the  $N \rightarrow \Delta$  and  $\Delta$  quadrupole FFs were able to quantify them. There is an ongoing effort by many groups to perform such simulations at pion masses approaching the physical value and reducing further lattice artifacts.

The theoretical foundations, experimental techniques, and lattice QCD simulation methods to access hadron

deformation through the measurement of quadrupole FFs are well established now. We can therefore expect in the near future that a refinement of the lattice calculations as well as new high-precision experiments with polarized beams and polarized targets, will allow to further sharpen our understanding of hadron shapes.

### Acknowledgements

The work of C.A. is partly supported by the Cyprus Research Promotion Foundation, of C.N.P. by the Ministry of Education, Greece and the Cyprus Institute, and of M.V. by the Research Center “Elementary Forces & Mathematical Foundations” at Mainz University.

We like to thank A. Bernstein, C. Carlson, D. Drechsel, P. Hoyer, Th. Korzec, G. Koutsou, C. Lorcé, V. Pascalutsa, S. Stiliaris N. Sparveris, L. Tiator, and A. Tsapalis, for useful discussions and correspondence.

- 
- [1] G. Gabrielse, D. Hanneke, T. Kinoshita, M. Nio, B. C. Odom, Phys. Rev. Lett. **97**, 030802 (2006).
  - [2] P. J. Mohr, B. N. Taylor, D. B. Newell, Rev. Mod. Phys. **80**, 633 (2008) [CODATA 2006].
  - [3] C. N. Papanicolas and A. M. Bernstein, *Shapes of Hadrons*, AIP Conf. Proc. **904**, 1 (2007), ISBN 978-0-7354-0411-3.
  - [4] R. Hofstadter, Rev. Mod. Phys. **28**, 214 (1956); R. Hofstadter, F. Bumiller and M.R. Yearian, Rev. Mod. Phys. **30**, 482 (1958).
  - [5] J. M. B. Kellogg, I. I. Rabi, N. F. Ramsey and J. R. Zacharias, Phys. Rev. **55**, 318 (1939).
  - [6] E. Gerjuoy and J. Schwinger, Phys. Rev. **61**, 138 (1942).
  - [7] P. Brix, Naturwiss. **64**, 293 (1977).
  - [8] F. W. Hersman *et al.*, Phys. Rev. C **33**, 1905 (1986).
  - [9] D. Bohle, A. Richter, W. Steffen, A. E. L. Dieperink, N. Lo Iudice, F. Palumbo and O. Scholten, Phys. Lett. B **137**, 27 (1984).
  - [10] D. Guéry-Odelin and S. Stringari, Phys. Rev. Lett. **83**, 4452 (1999).
  - [11] O.M. Maragò, S.A. Hopkins, J. Arlt, E. Hodby, G. Hechenblaikner, and C.J. Foot, Phys. Rev. Lett. **84**, 2056 (2000).
  - [12] S. L. Glashow, Physica A **96**, 27 (1979).
  - [13] A. De Rujula, H. Georgi and S. L. Glashow, Phys. Rev. D **12**, 147 (1975).
  - [14] W. Heisenberg, Z. Phys. **39**, 499 (1926); G. Breit, Phys. Rev. **36**, 383 (1930), and E. Fermi, Z. Phys. **60**, 320 (1930).
  - [15] N. Isgur, G. Karl and R. Koniuk, Phys. Rev. D **25**, 2394 (1982).
  - [16] R. D. Carlitz, S. D. Ellis and R. Savit, Phys. Lett. B **68**, 443 (1977).
  - [17] N. Isgur, Acta Phys. Polon. B **8**, 1081 (1977).
  - [18] N. Isgur, G. Karl and D. W. L. Sprung, Phys. Rev. D **23**, 163 (1981).
  - [19] S. D. Drell and T. M. Yan, Phys. Rev. Lett. **24**, 181 (1970).
  - [20] L. Susskind, Phys. Rev. **165**, 1547 (1968).
  - [21] M. Burkardt, Phys. Rev. D **62**, 071503 (2000); Int. J. Mod. Phys. A **18**, 173 (2003).
  - [22] G. A. Miller, Phys. Rev. Lett. **99**, 112001 (2007).
  - [23] C. E. Carlson and M. Vanderhaeghen, Phys. Rev. Lett. **100**, 032004 (2008).
  - [24] C. E. Carlson and M. Vanderhaeghen, Eur. Phys. J. A **41**, 1 (2009).
  - [25] C. Lorcé, Phys. Rev. D **79**, 113011 (2009).
  - [26] M. Järvinen, Phys. Rev. D **71**, 085006 (2005).
  - [27] P. Hoyer, arXiv:0909.3045 [hep-ph].
  - [28] S. Ferrara, M. Porrati and V. L. Telegdi, Phys. Rev. D **46**, 3529 (1992).
  - [29] K. Hagiwara, R. D. Peccei, D. Zeppenfeld and K. Hikasa, Nucl. Phys. B **282**, 253 (1987).
  - [30] Nakamura *et al.* [ Particle Data Group Collaboration ], J. Phys. G **G37**, 075021 (2010).
  - [31] T. E. O. Ericson and M. Rosa-Clot, Nucl. Phys. A **405**, 497 (1983).
  - [32] D. Abbott *et al.* [JLAB t20 Coll.], Eur. Phys. J. A **7**, 421 (2000).
  - [33] M. Kotulla [TAPS/A2 Collaboration], Prog. Part. Nucl. Phys. **50**, 295 (2003).
  - [34] C. Alexandrou *et al.*, PoS **LAT2009**, 155 (2009).
  - [35] C. Alexandrou and G. Koutsou, Phys. Rev. D **78**, 094506 (2008).
  - [36] J. N. Hedditch *et al.*, Phys. Rev. D **75**, 094504 (2007).
  - [37] C. N. Papanicolas *et al.*, Phys. Rev. Lett. **54**, 26 (1985).
  - [38] D. Drechsel, S. S. Kamalov and L. Tiator, Eur. Phys. J. A **34**, 69 (2007).
  - [39] T. Sato and T.-S.H. Lee, Phys. Rev. C **54**, 2660 (1996); *ibid.* **63**, 055201 (2001).
  - [40] S. S. Kamalov and S. N. Yang, Phys. Rev. Lett. **83**, 4494 (1999); S. S. Kamalov, S. N. Yang, D. Drechsel, O. Hanstein, and L. Tiator, Phys. Rev. C **64**, 032201(R) (2001).

- [41] K. Wilson, Phys. Rev. D **10**, 245 (1974).
- [42] K. Jansen, PoS **LATTICE2008** (2008) 010, and references therein.
- [43] S. Dürr *et al.*, Science **322**, 1224 (2008); S. Dürr *et al.*, arXiv:1011.2711 [hep-lat].
- [44] C. Alexandrou *et al.*, Phys. Rev. D **80**, 114503 (2009).
- [45] Ph. Hagler, Phys. Rept. **490**, 49 (2010).
- [46] M. Göckeler *et al.*, Phys. Rev. Lett. **98**, 222001 (2007).
- [47] D. Brommel *et al.* [QCDSF Coll. and UKQCD Coll.], Phys. Rev. Lett. **101**, 122001 (2008).
- [48] C. Alexandrou *et al.*, Phys. Rev. D **79**, 014507 (2009); C. Alexandrou *et al.*, Nucl. Phys. A **825**, 115 (2009).
- [49] M. Lüscher, Nucl. Phys. B **364**, 237 (1991); *ibid* **354**, 531 (1991);
- [50] C. Aubin, K. Orginos, V. Pascalutsa and M. Vanderhaeghen, Phys. Rev. D **79**, 051502 (2009).
- [51] I. K. Bensafa *et al.* [MAMi-A1 Coll.], Eur. Phys. J. A **32**, 69 (2007).
- [52] N. F. Sparveris *et al.*, Phys. Rev. C **78**, 018201 (2008).
- [53] C.N. Papanicolas, in Proceedings of the *Workshop on Excited Baryons*. Editors : G. Adams, N. Mukhopadhyay, and P. Stoler, World Scientific, Singapore, 1989.
- [54] L. D. van Buuren *et al.*, Phys. Rev. Lett. **89**, 012001 (2002).
- [55] J. J. Kelly *et al.* [Jefferson Lab Hall A Coll.], Phys. Rev. Lett. **95**, 102001 (2005).
- [56] M. Kotulla [CBELSA/TAPS Collaboration], Int. J. Mod. Phys. A **20** (2005) 690.
- [57] R. Beck *et al.*, Phys. Rev. Lett. **78**, 606 (1997);
- [58] G. Blanpied *et al.*, Phys. Rev. Lett. **79**, 4337 (1997); Phys. Rev. C **64**, 025203 (2001).
- [59] G. Galler *et al.*, Phys. Lett. B **503**, 245 (2001).
- [60] R. A. Arndt *et al.*, arXiv:nucl-th/0106059.
- [61] M. Kotulla, AIP Conf. Proc. **904** (2007) 203.
- [62] H. Merkel, Eur. Phys. J. A **28S1** (2006) 129.
- [63] M. Kotulla *et al.*, Phys. Rev. Lett. **89** (2002) 272001.
- [64] F. Kalleicher *et al.*, Z. Phys. A **359** (1997) 201.
- [65] G. A. Warren *et al.* [M.I.T.-Bates OOPS Coll. and FPP Coll.], Phys. Rev. C **58**, 3722 (1998).
- [66] V. V. Frolov *et al.*, Phys. Rev. Lett. **82**, 45 (1999).
- [67] C. Mertz *et al.*, Phys. Rev. Lett. **86**, 2963 (2001).
- [68] T. Pospischil *et al.*, Phys. Rev. Lett. **86**, 2959 (2001).
- [69] C. Kunz *et al.* [MIT-Bates OOPS Coll.], Phys. Lett. B **564**, 21 (2003).
- [70] K. Joo *et al.* [CLAS Coll.], Phys. Rev. Lett. **88**, 122001 (2002).
- [71] N. F. Sparveris *et al.* [OOPS Coll.], Phys. Rev. Lett. **94**, 022003 (2005).
- [72] D. Elsner *et al.*, Eur. Phys. J. A **27**, 91 (2006).
- [73] S. Stave *et al.*, Eur. Phys. J. A **30**, 471 (2006).
- [74] M. Ungaro *et al.* [CLAS Coll.], Phys. Rev. Lett. **97**, 112003 (2006).
- [75] N. F. Sparveris *et al.*, Phys. Lett. B **651**, 102 (2007).
- [76] S. Stave *et al.* [A1 Coll.], Phys. Rev. C **78**, 025209 (2008).
- [77] J. M. Kirkpatrick *et al.*, arXiv:0810.4563 [nucl-ex].
- [78] J. Mandeville *et al.*, Phys. Rev. Lett. **72** (1994) 3325.
- [79] N. F. Sparveris, AIP Conf. Proc. **904** (2007) 213.
- [80] P. L. Cole [CLAS Collaboration], AIP Conf. Proc. **904** (2007) 203.
- [81] A.M. Bernstein, Eur. Phys. J. A **17**, 349 (2003).
- [82] C. E. Carlson, Phys. Rev. D **34**, 2704 (1986).
- [83] B. Pasquini, M. Gorchtein, D. Drechsel, A. Metz and M. Vanderhaeghen, Eur. Phys. J. A **11**, 185 (2001).
- [84] C. Papanicolas, Eur. Phys. J. A **18**, 141 (2003).
- [85] S. Stave, A. M. Bernstein and I. Nakagawa, AIP Conf. Proc. **904**, 245 (2007).
- [86] E. Stiliaris and C. N. Papanicolas, AIP Conf. Proc. **904**, 257 (2007) and to be published.
- [87] C. Alexandrou, C. N. Papanicolas and E. Stiliaris, PoS **LATTICE2008**, 099 (2008).
- [88] S. Nozawa and D. B. Leinweber, Phys. Rev. D **42**, 3567 (1990).
- [89] V. Pascalutsa, M. Vanderhaeghen and S. N. Yang, Phys. Rept. **437**, 125 (2007).
- [90] C. W. Bernard *et al.*, Phys. Rev. D **64**, 054506 (2001).
- [91] H. F. Jones and M. D. Scadron, Ann. Phys. **81**, 1 (1973).
- [92] L. Tiator, D. Drechsel, S. S. Kamalov and S. N. Yang, Eur. Phys. J. A **17**, 357 (2003).
- [93] N. Isgur and G. Karl, Phys. Rev. D **18**, 4187 (1978); *ibid.* D **19**, 2653 (1979); *ibid.* D **20**, 1191 (1979).
- [94] A. De Rujula, H. Georgi and S. L. Glashow, Phys. Rev. D **12**, 147 (1975).
- [95] R. Koniuk and N. Isgur, Phys. Rev. D **21**, 1868 (1980).
- [96] S. S. Gershtein and G. V. Jikia, Sov. J. Nucl. Phys. **34**, 870 (1981); M. Bourdeau and N. C. Mukhopadhyay, Phys. Rev. Lett. **58**, 976 (1987); Sov. J. Nucl. Phys. **45**, 674 (1987).
- [97] D. Drechsel and M. M. Giannini, Phys. Lett. B **143**, 329 (1984).
- [98] M. M. Giannini, Rept. Prog. Phys. **54**, 453 (1990).
- [99] S. Capstick and G. Karl, Phys. Rev. D **41**, 2767 (1990); S. Capstick, Phys. Rev. D **46**, 2864 (1992).
- [100] G. Kaelbermann and J. M. Eisenberg, Phys. Rev. D **28**, 71 (1983).
- [101] K. Bermuth, D. Drechsel, L. Tiator and J. B. Seaborn, Phys. Rev. D **37**, 89 (1988).
- [102] J. F. Donoghue, E. Golowich and B. R. Holstein, Phys. Rev. D **12**, 2875 (1975).
- [103] A. W. Thomas, Adv. Nucl. Phys. **13**, 1 (1984).
- [104] D. H. Lu, A. W. Thomas and A. G. Williams, Phys. Rev. C **55**, 3108 (1997).
- [105] A. Wirzba and W. Weise, Phys. Lett. B **188**, 6 (1987); A. Abada, H. Weigel and H. Reinhardt, Phys. Lett. B **366**, 26 (1996);
- [106] H. Walliser and G. Holzwarth, Z. Phys. A **357**, 317 (1997).
- [107] T. Watabe, C. V. Christov and K. Goeke, Phys. Lett. B **349**, 197 (1995).
- [108] A. Silva, D. Urbano, T. Watabe, M. Fiolhais and K. Goeke, Nucl. Phys. A **675**, 637 (2000); T. Ledwig, A. Silva and M. Vanderhaeghen, Phys. Rev. D **79**, 094025 (2009).
- [109] A. J. Buchmann, E. Hernandez and A. Faessler, Phys. Rev. C **55**, 448 (1997).
- [110] A. Faessler *et al.*, Phys. Rev. D **74**, 074010 (2006).
- [111] G. 't Hooft, Nucl. Phys. B **72**, 461 (1974).
- [112] E. Witten, Nucl. Phys. B **160**, 57 (1979).
- [113] E. Jenkins, Ann. Rev. Nucl. Part. Sci. **48**, 81 (1998).
- [114] R. F. Lebed, Czech. J. Phys. **49**, 1273 (1999).
- [115] E. Jenkins and A. V. Manohar, Phys. Lett. B **335**, 452 (1994).
- [116] E. Jenkins, X. d. Ji and A. V. Manohar, Phys. Rev. Lett. **89**, 242001 (2002).
- [117] A. J. Buchmann, J. A. Hester and R. F. Lebed, Phys. Rev. D **66**, 056002 (2002).
- [118] V. Pascalutsa and M. Vanderhaeghen, Phys. Rev. D **76**, 111501 (2007).

- [119] P. Grabmayr and A. J. Buchmann, Phys. Rev. Lett. **86**, 2237 (2001); A. J. Buchmann, Phys. Rev. Lett. **93**, 212301 (2004).
- [120] C. Allton *et al.* [RBC-UKQCD Coll.], Phys. Rev. D **78**, 114509 (2008).
- [121] C. Alexandrou, G. Koutsou, J. W. Negele, Y. Proestos and A. Tsapalis, Phys. Rev. D **83**, 014501 (2011).
- [122] W. Bartel *et al.*, Phys. Lett. B **28**, 148 (1968); J. C. Alder *et al.*, Nucl. Phys. B **46**, 573 (1972); K. Bätzner *et al.*, Phys. Lett. B **39**, 575 (1972); S. Stein *et al.*, Phys. Rev. D **12**, 1884 (1975).
- [123] C. Alexandrou *et al.*, Phys. Rev. D **77**, 085012 (2008).
- [124] S. Weinberg, Physica A **96**, 327 (1979).
- [125] J. Gasser and H. Leutwyler, Annals Phys. **158**, 142 (1984); Nucl. Phys. B **250**, 465 (1985).
- [126] V. Bernard, N. Kaiser, and U. G. Meißner, Int. J. Mod. Phys. E **4**, 193 (1995).
- [127] M. N. Butler, M. J. Savage and R. P. Springer, Phys. Lett. B **304**, 353 (1993).
- [128] G. C. Gellas, T. R. Hemmert, C. N. Ktorides and G. I. Poulis, Phys. Rev. D **60**, 054022 (1999).
- [129] T. A. Gail and T. R. Hemmert, Eur. Phys. J. A **28**, 91 (2006).
- [130] V. Pascalutsa and D. R. Phillips, Phys. Rev. C **67**, 055202 (2003).
- [131] V. Pascalutsa and M. Vanderhaeghen, Phys. Rev. Lett. **95**, 232001 (2005); Phys. Rev. D **73**, 034003 (2006).
- [132] C. Alexandrou *et al.*, Phys. Rev. Lett. **94**, 021601 (2005).